Design and Mechanical Validation of Commercially Viable, Personalized Passive Prosthetic Feet

by

Charlotte Méry Folinus

Submitted to the Department of Mechanical Engineering
in partial fulfillment of the requirements for the degree of

Master of Science in Mechanical Engineering

at the

MASSACHUSETTS INSTITUTE OF TECHNOLOGY

May 2022

Author .....
Department of Mechanical Engineering
May 6, 2022

Certified by .....
Amos G. Winter, V
Ratan N. Tata Associate Professor of Mechanical Engineering
Thesis Supervisor

Accepted by .....
Nicolas Hadjiconstantinou
Professor of Mechanical Engineering
Graduate Officer

Design and Mechanical Validation of Commercially Viable, Personalized Passive Prosthetic Feet

by

Charlotte Méry Folinus

Submitted to the Department of Mechanical Engineering
on May 6, 2022, in partial fulfillment of the
requirements for the degree of
Master of Science in Mechanical Engineering

Abstract

Existing energy storage and return (ESR) prosthetic feet are available in a low-resolution and discrete set of size and stiffness options. While these devices are reimbursed for thousands of dollars through insurance, the current low-resolution sizing systems may limit the walking performance of many amputees. The design, manufacturing, and provision processes used to create existing prosthetic feet are inherently low resolution; providing amputee-specific personalization with these methods is either not possible or not commercially viable. The Lower Leg Trajectory Error (LLTE) design framework provides an oportunity for designing high-performance, amputee-specific prosthetic feet; however, previous foot prototypes were designed as experimental prototypes to demonstrate the LLTE theory, not to satisfy the economic, mechanical, and aesthetic requirements necessary for commercial adoption.

This thesis aims to understand how a personalized, affordable prothetic foot can be realized for a clinical-commercial setting. First, we evaluate stakeholder needs and identify the flows of products, capital, and services between prosthetics suppliers, distributors, prosthetists, amputees, and insurance providers. We elucidate the design requirements for a personalized prosthetic foot that can be manufactured, distributed, and clinically provided by Hanger, a current leader in both product distribution and patient care in orthotics and prosthetics.

Based on material properties and manufacturing process capabilities, we demonstrate why CNC machining of Nylon 6/6 is an appropriate process for satisfying these requirements. Although additive manufacturing is often seen as a compelling method for creating customized products, additively manufactured ESR prosthetic feet would likely have inferior walking performance, take longer to produce, cost more, and experience greater manufacturing variability than CNC machined feet. Next, this thesis presents a novel parametric foot architecture that can be CNC machined, fits within a commercial foot shell, and can be designed for individual users' body characteristics and activity levels. Lastly, we demonstrate that prototypes made using the upgraded foot design mechanically behave as anticipated and satisfy industry-standard strength and mechanical performance requirements.

Thesis Supervisor: Amos G. Winter, V
Title: Ratan N. Tata Associate Professor of Mechanical Engineering

Acknowledgments

It has taken a village of people to get me to and through this chapter of my life, and I am eternally grateful to each of you for your roles, both big and small.

My advisor, Prof. Amos Winter, decided to start this journey together days before MIT shut down in Spring 2020. At the time, neither of us could have predicted how the world would change, how this project would evolve, or how I would grow in the following two years. Amos, you have always believed in me and seen the best in me, giving me patience I did not always deserve. Thank you for constantly challenging me to grow as an engineer, researcher, and person. My undergraduate advisor, Prof. Peko Hosoi, helped me realize an enthusiasm for research and encouraged me to stick around MIT as a graduate student. Thank you for sharing your contagious curiosity and helping me realize the joy of using simple physics to interpret the world around me.

Our team of collaborators at Hanger not only financially supported this work, but they more importantly gave me interesting and impactful design challenges. Dr. Aaron Flores, Phil Stevens, Antonio Diaz, Chris Mowrer, and Erin O'Brien, thank you for providing answers to questions I never thought to ask and keeping me grounded in your real-world needs and experiences. Thank you to Dwiesha, Lara, and Vahness for helping me navigate IRBs and order countless prosthetic components, to Quincey and Jessica for on-the-ground support and hiking recommendations in Utah, and to the countless others at Hanger who helped make this work possible.

The Pappalardo and LMP shop staff supported both my hardware and sanity for much of the last five years. You have fostered a lifelong love of hands-on engineering, a curiosity to learn, and an enthusiasm to share my work with others. A special thanks goes to Dr. Daniel Braunstein, who has been a sounding board for more design and life challenges than he probably bargained for. Danny, you encourage me to have greater balance, to prioritize the things that truly matter, and to grow to become the best version of myself. While I "could have gone to graduate school somewhere with more sunshine," I am deeply grateful to be here and able to wander over to

Pappalardo like a stray cat to visit. I owe you a windlass and a sticky bun.

The GEAR prosthetics team has always helped me put my best foot forward. Victor, Heidi, and Nina welcomed me to grad school during a difficult virtual year with laughter, patience, and curiosity. Victor, thank you for being an amazing mentor; I feel so fortunate to have learned so much from you about design, prosthetic feet, grad school, and windsurfing. Thank you also to Uriel and Rosalie, my undergraduate research assistants, for your contributions, enthusiasm, and thoughtful questions. To the entire GEAR lab, thank you for your support and our many goofy memories together.

MakerWorkshop was one of the first shops I worked in as an undergraduate. At first, it was just a physical place to prototype and fabricate, but I grew to find a community of designers, tinkerers, and friends. This work would not have been possible without the people and resources of MakerWorkshop. Thank you to Victor for giving me my first machine training five years ago and to all of the shiftmates and mentors through the years who have taught me things, made me laugh, and provided design and life advice.

I owe thanks as well to a few folks at home who played important roles in getting me here in the first place. Genie Beaver and Amy Eubanks, thank you for inspiring me as a runner and being some of the first to make me excited about biomechanics and shoes. You helped put me on an exciting path that has evolved significantly over the years and taken me across the country and around the world. Nurfatimah Merchant, thank you for teaching me the beauty in math, calculus, and parametric curves. Thank you also for writing my undergraduate recommendations even when I asked on the last possible day, because "you'll probably be a mechanical engineer or something." I guess you were right.

I would be nowhere without the support of my family. They instilled an early love of math and science and continue to support me every step of the way. My godparents, Kate and Jerry, encouraged me to have fun with all that I do. Kate, thank you for being a true fairy godmother, keeping me well supplied with new recipes, good chocolate, silly shirts, and reminders to never take things too seriously. Jerry, thank

you for your stubbornness, showing me the power of numbers and statistics, and our many runs together. I think you'd be proud of where I am. My parents, Marilyn and Jeffrey, taught me to be curious, strive for excellence, and to challenge myself. Thank you for showing me the value of perseverance while also reminding me to take a step back to reflect. You encourage me to find and follow my dreams, to take adventures, and to trust that life will fall well enough into place if I do what I love. Thank you.

Here's to the next chapter and the many adventures ahead.

You cannot understand good design
if you do not understand people;
Design is made for people.

Dieter Rams

Contents

1 Introduction **15**

1.1 Motivation for commercial, amputee-specific personalized prosthetic feet 15

1.2 Opportunities and the Lower Leg Trajectory Error framework 18

1.3 Thesis objectives and outline 21

2 Stakeholder needs and design requirements **31**

2.1 Overview of key stakeholders 32

2.2 Design requirements 35

3 Material and manufacturing process selection **45**

3.1 Candidate materials 45

3.2 Manufacturing rate, cost, and quality 49

3.2.1 Rate comparison 49

3.2.2 Cost comparison 50

3.2.3 Quality comparison 54

3.3 Justification of chosen material and manufacturing process 56

3.4 Supplementary information 56

3.4.1 Relationship between material performance indices and LLTE 56

3.4.2 Relative strength of more complex cross sections 58

3.4.3 Cost model implementation 65

4 Foot form: improvements to meet commercial requirements **83**

4.1 Parametric model of foot architecture 84

4.2 Constitutive model and design optimization 87
4.3 Performance characterization 89
4.4 Supplementary information 90
4.4.1 Determination of permissible foot envelope 90
4.4.2 Detailed implementation of optimization problem 92

5 Mechanical validation **99**
5.1 Mechanical testing of prototype foot stiffness 99
5.2 ISO ultimate strength mechanical testing 101
5.3 AOPA dynamic heel and keel testing 103

6 Discussion and Conclusions **109**
6.1 Discussion 109
6.2 Next Steps 112
6.2.1 Opportunities for Future Work 112
6.2.2 Remaining Knowledge Gaps 117

List of Figures

1-1 Diagram of the LLTE framework 19

2-1 Stakeholder flow diagram 32

3-1 Material performance indices 47
3-2 Cost breakdown for CNC machining 53
3-3 Manufacturing cost comparison 54
3-4 LLTE scores and material performance indices for example materials 58
3-5 Diagram of single- and multi-material cross sections 59
3-6 Overview of Markforged CFF process 59
3-7 Relative strength vs. area fraction for laminated composites 62
3-8 Relative strength vs. fiber thickness for laminated composites 63
3-9 Cross section geometries 63
3-10 Relative strength for multiple cross section geometries 65
3-11 Demonstration of model sensitivity to input parameters 73
3-12 Cost breakdown for Markforged CFF 74
3-13 Cost breakdown for HP MJF 74

4-1 Comparison of previous and upgraded foot geometries 84
4-2 Parametric model of upgraded foot architecture 85
4-3 Foot-shell-shoe constitutive model 88
4-4 Performance of upgraded foot architecture across range of body sizes 90

5-1 Constitutive model testing experimental setup 100
5-2 Load-displacement curve of constitutive model testing 101

5-3 ISO ultimate static strength testing experimental setup 102
5-4 Load-displacement curves from ISO ultimate static strength testing . 103
5-5 AOPA dynamic keel experimental setup 104
5-6 Load-displacement curves from AOPA dynamic heel and dynamic keel testing 105

6-1 LLTE block diagram and opportunities for improvement 113

List of Tables

2.1 Core design requirements 36

3.1 Optimization setup parameters 57
3.2 Overall production parameters used for all processes 69
3.3 Markforged CFF-specific process parameters used as model inputs . . 70
3.4 HP MJF-specific process parameters used as model inputs 71
3.5 CNC machining-specific process parameters used as model inputs . . 72

4.1 Body size parameters used to optimize prosthetic feet for a range of target users 89
4.2 Design variable upper and lower bounds 94

Chapter 1

Introduction

1.1 Motivation for commercial, amputee-specific personalized prosthetic feet

Existing energy storage and return (ESR) prosthetic feet are available in a discrete and low-resolution set of size and stiffness options, which may leave many users with limited walking performance. Many existing prosthetic foot models are available in ~ 5 stiffness categories in a given foot length [1–5], giving a size-to-size variation in stiffness of approximately 10-20% [6–8]. The measured size-to-size stiffness variation may not be consistent between foot lengths, models, or manufacturers [6, 8], and it is greater than both users' stiffness perception ($\sim 5-10\%$ [9]) and repeatability of stiffness preference ($\sim 5\%$ [10]) when walking in a variable-stiffness prosthetic foot. This suggests that users may reliably make foot preference selection with a higher resolution than facilitated by existing sizing systems. User stiffness preference may be associated with clinically relevant improvements to gait, such as improved symmetry [11].

Although the existing size and stiffness categories work well for many users, they may leave out certain types of users or demographics, who fall outside of height, weight, and mobility norms, particularly women, children, and military personnel [12, 13]. Women often use devices primarily designed for men; as a result, they

may be too large or stiff or not designed to accommodate common female footwear [12, 14, 15]. Compared with others of the same body size, children and military personnel may have increased load requirements and thus require prosthetic components capable of withstanding the greater loads associated with their higher mobility activities such as walking on varied terrains, participating in recreational sports, or carrying heavy loads. The size and stiffness mismatch between amputees and existing prosthetic feet results in negative clinical and subjective outcomes due to increased gait compensation, long-term injuries, and pain [16–18].

Current prosthetic foot design, manufacturing, and provision processes are inherently low-resolution. Providing a greater level of personalization with these techniques is either not possible or not commercially viable. Existing prosthetic foot design methods require iteration and extensive user testing [19]. This empirical approach decreases the potential resolution of ESR foot sizes. Existing stiffness categories often informally result from this user testing [10], not from a predictive design process. Without a deterministic design methodology, it is not possible to design amputee-specific prosthetic feet; designing a prosthetic foot for a specific amputee would require multiple rounds of user testing with that individual. The manufacturing of ESR feet also limits their potential for personalization. ESR foot manufacturing often utilizes expensive composite materials, such as carbon fiber or fiberglass, which require fixed tooling. Increasing the number of size and stiffness options requires investing in additional sets of tooling, directly increasing the manufacturing cost.

Prosthetic foot provision processes have co-evolved with the existing resolution of size and stiffness options. Fitting a prosthetic foot can be time-intensive and require many alignment iterations. To compensate for the low resolution of available stiffness options, prosthetists often make small adjustments to foot behavior by iteratively tuning alignment [20] or interchanging reconfigurable foot components. While these components, such as heel wedges and bumpers, may allow for adjustability beyond the coarse foot sizing system, they are still low-resolution. Heel wedges are often shipped with the prosthetic foot or available as a kit with multiple wedges. These interchangeable components are often available in "soft" and "firm" options, as with

the Fillauer AllPro [21] or "soft", "medium", and "firm" options. Shipping a higher-resolution set of components with many heel wedge options would result in wasted money to produce and ship unused items, and it could increase time requirements on prosthetists to select appropriate components. Additionally, heel wedges may have unpredictable, manufacturer-dependent effects [6]. The highly manual fitting process leverages clinical expertise but requires trial-and-error and significant time to converge on an appropriate prosthesis and alignment. Fully customizing a prosthetic foot cannot reasonably happen during fitting; additional fitting and alignment iterations might be perceived as cumbersome. Increasing the per-patient prosthetist time also comes at a cost; if a prosthetist is able to see fewer patients, they are able to generate less revenue.

A line of prosthetic feet that offers a high resolution set of size and stiffness options, designed through amputee-specific personalization, could provide clinical value through improved clinical outcome measures and walking performance. These outcome measures are often related to restoring functional mobility and quality of life [22–25], which is often seen as a primary goal of rehabilitation [22–24]. Quantitatively, improved walking performance can relate to reduced gait asymmetries, which are often associated with increased gait compensation and increased loading on the intact leg, which can result in long-term overuse. By reducing gait compensation and the risks of related long-term overuse injuries such as osteoarthiritis [16, 26], personalized prosthetic devices also have the potential to provide economic value by reducing the overall cost of long-term injuries. This is of particular interest in the United States, where healthcare costs are among the highest in the world [27–30], lifetime prosthetic care for a unilateral transtibial amputee costs approximately one million USD [31], and there is a growing desire to reduce costs through evidence-based prescription practices [32] and amputee-independent metrics [33].

To be commercially viable, a personalized prosthetic foot must balance the clinical benefits of customization with the functional requirements of the clinical-commercial ecosystem, utilize manufacturing processes which facilitate personalization, and be designed with a form factor and using a design methodology which satisfies these

requirements. Despite the promise of personalization, a prosthetic foot which is only personalizable but not also commercially viable will not gain traction as a commercial product. Increasing device personalization also increases the complexity of manufacturing and distribution, but it need not imply full customization and an infinite number of potential foot designs. Infinite customization may be neither clinically necessary nor commercially advantageous; a finite, but high-resolution set of variants may provide sufficient personalization while balancing distribution complexity.

The requirements for a commercially-viable, patient-specific prosthetic foot are unknown. There is a growing desire to use digital manufacturing processes such as additive manufacturing (AM) to produce patient-specific medical devices [34]; however, existing prosthetic design processes are empirical, iterative [10, 19, 35–37], and too slow to facilitate customization. AM is certainly a promising solution for creating personalized medical devices [34] such as prosthetic feet [38–42]; howerver, its process capabilities, part-to-part variability, and achievable material properties introduce additional uncertainty. It is not known whether AM is the most appropriate way to manufacture personalized prosthetic feet.

1.2 Opportunities and the Lower Leg Trajectory Error framework

A manufacturing process capable of producing a high-resolution set of prosthetic foot size and stiffness options must be paired both with a design methodology which facilitates personalization and with an appropriate embodiment of foot geometry. The lower leg trajectory error (LLTE) design framework [43] provides a quantitative methodology for prosthetic foot design by connecting the mechanical design of a prosthetic foot with its anticipated biomechanical performance (Fig. 1-1). The LLTE methodology leverages a parametric model of a prosthetic foot which describes the foot's geometry, a constitutive model to predict its behavior throughout stance, and the LLTE metric, which quantifies how well the prosthetic foot enables an amputee

to replicate target kinematics when reference loads are applied.

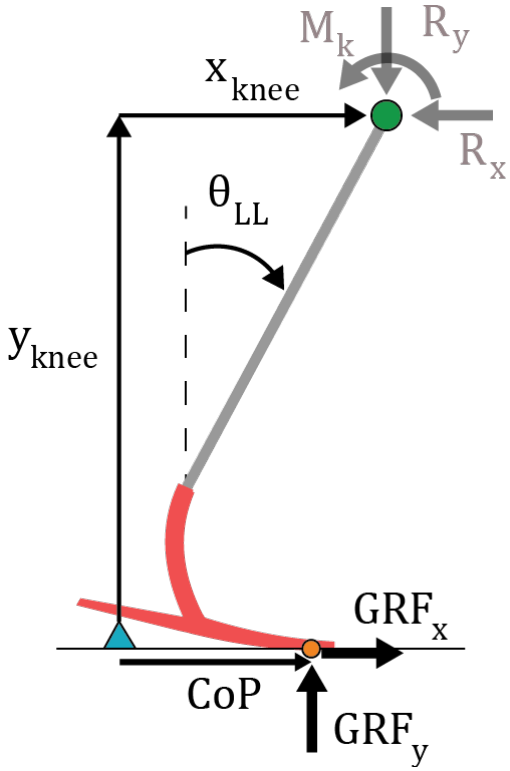

Figure 1-1: Diagram of the LLTE design framework, shown with force and moment balance analysis in the sagittal plane. The position and orientation of the lower leg segment is defined by the position of the knee (x_{knee}, y_{knee}) and the angle of the lower leg segment θ_{LL}. These coordinates are calculated from the deformed shape of the prosthetic foot under prescribed loading conditions (GRF_x and GRF_y at a specific CoP).

Specifically, the deformation of the prosthetic foot is used to compute the resulting lower leg trajectory when target reference loads (ground reaction forces, GRFs, applied at the corresponding centers of pressure, CoPs) are applied at each individual frame n (time instance throughout stance) of N total frames (Fig. 1-1). The LLTE metric quantifies the foot's biomechanical performance throughout stance as the average deviation (i.e. error) between the calculated prosthetic side lower leg trajectory and the target reference lower leg trajectory:

$$\text{LLTE} = \left[\frac{1}{N} \sum_{n=1}^{N} \left\{ \left(\frac{x_{\text{knee,n}}^{\text{model}} - x_{\text{knee,n}}^{\text{ref}}}{L_{\text{lowerleg}}} \right)^2 + \left(\frac{y_{\text{knee,n}}^{\text{model}} - y_{\text{knee,n}}^{\text{ref}}}{L_{\text{lowerleg}}} \right)^2 + \left(\frac{\theta_{\text{LL,n}}^{\text{model}} - \theta_{\text{LL,n}}^{\text{ref}}}{\text{atan}(\frac{L_{\text{lowerleg}}}{\text{L}_{\text{foot}}})} \right)^2 \right\} \right]^{\frac{1}{2}}, \tag{1.1}$$

where the superscripts "model" and "ref" correspond to the values computed from the constitutive model and those from the reference data set, respectively. The deviations from each reference variable are normalized by the lower leg length L_{lowerleg} and $\text{atan}(\frac{L_{\text{lowerleg}}}{L_{\text{foot}}})$. The lower the LLTE value is, the more closely the prosthetic foot enables replication of the target walking pattern; the LLTE-optimal design is that which best enables this replication.

The LLTE metric can be incorporated in an optimization to systematically adjust the mechanical properties (geometry and stiffness) of a prosthetic foot, resulting in foot designs which minimize the LLTE value [43] and yield a desired biomechanical response [43, 44]. This facilitates amputee-specific personalization, or design of a prosthetic foot based on an individual's body size and activity level [43–47]. In prior gait testing, LLTE feet were customized for users with a range of body sizes [45, 46], were manufactured from Nylon 6/6, and showed similar or better biomechanical performance and subjective ratings than commercially-available, carbon fiber ESR prosthetic feet [45]. The LLTE methodology is also capable of producing prosthetic feet which meet commercial strength standards such as ISO 10328 [47, 48] and which survive extended use in rugged conditions [49].

Despite the promise of the LLTE methodology, prior LLTE-designed prosthetic feet were created to validate the LLTE design framework, not specifically to meet requirements for commercialization. Prior prototypes had simple form factors which could be fabricated using a waterjet and two-axis milling machine [44–47, 50, 51]. To minimize gait variation due to footwear [52] during biomechanical testing, these prototypes were designed to be worn overground. As a result, they did not fit within

commercial foot shells, which is the typical form factor for ESR feet, and the constitutive model of prosthesis behavior did not consider the additional compliance introduced by a foot shell or shoe.

1.3 Thesis objectives and outline

The overall goal of this thesis is to use the LLTE framework to create commercially viable, personalized prosthetic feet. The outline of the thesis is as follows:

Chapter 2: Stakeholder needs and design requirements

This chapter elucidates the economic, mechanical, and aesthetic requirements that must be met for a commercially viable, personalized prosthetic foot. First, key stakeholders in the manufacturing, distribution, and provision of a custom prosthetic foot are introduced and related to each other through the flows of products, services, and capital. Next, these flows are used to outline core requirements from each stakeholder and to justify a set of design requirements for the commercially viable, personalized prosthetic foot.

Chapter 3: Material and manufacturing process selection

This chapter compares the suitability of candidate materials and manufacturing processes for creating personalized prosthetic feet. Materials are evaluated according to their strength and energy storage potential, and manufacturing processes are assessed by their estimated production rate, cost, and quality. CNC machining of Nylon 6/6 is identified as the most appropriate material-process combination for satisfying the design requirements in Chap. 2.

Chapter 4: Foot form: improvements to meet commercial requirements

This chapter presents a novel parametric foot architecture which satisfies commercial economic, mechanical, and aesthetic requirements. The constitutive model and optimization scheme implementations are also introduced here. The upgraded foot

geometry is used to design customized prosthetic feet for amputees with a range of body sizes.

Chapter 5: Mechanical validation

This chapter discusses experimental testing used to demonstrate that the upgraded foot designs mechanically behave as predicted and satisfy mechanical requirements outlined in Chap. 2.

Chapter 6: Discussion and conclusions

The results from this thesis are synthesized, and implications of this work are discussed. This chapter also presents opportunities for future work toward commercialization as well as remaining knowledge gaps for additional research.

Bibliography

[1] Fillauer. Lower Extremity Prosthetics Product Catalog, 2020. URL `fillauer.com`.

[2] Freedom Innovations. Lower Limb Prosthetic Solutions Product Catalog, 2015.

[3] Össur. Prosthetic Solutions Catalogue, 2016.

[4] Ottobock. Prosthetics - Lower limbs, 2015.

[5] Endolite North America. Catalog 2016/2017 - Lower limb prosthetic product range, 2016.

[6] Nicholas D. Womac, Richard R. Neptune, and Glenn K. Klute. Stiffness and energy storage characteristics of energy storage and return prosthetic feet. *Prosthetics and Orthotics International*, 43(3):266–275, 2019. ISSN 17461553. doi: 10.1177/0309364618823127.

[7] Heidi V Peterson. *Design of a Novel Mechatronic System to Test Prosthetic Feet Under Specific Walking Activity Loads and Evaluate their Lower Leg Trajectory Error*. PhD thesis, Massachusetts Institute of Technology, 2021.

[8] Anne T Turner, Elizabeth G Halsne, Joshua M Caputo, Carl S Curran, Andrew H Hansen, Brian J Hafner, and Morgenroth. Prosthetic forefoot and heel stiffness across consecutive foot stiffness categories and sizes. *PLoS ONE*, 17(5):e0268136, 2022. doi: 10.1371/journal.pone.0268136. URL `http://dx.doi.org/10.1371/journal.pone.0268136`.

[9] Max K. Shepherd, Alejandro F. Azocar, Matthew J. Major, and Elliott J. Rouse. Amputee perception of prosthetic ankle stiffness during locomotion. *Journal of NeuroEngineering and Rehabilitation*, 15(1), 2018. ISSN 17430003. doi: 10.1186/s12984-018-0432-5. URL `https://doi.org/10.1186/s12984-018-0432-5`.

[10] Max K. Shepherd and Elliott J. Rouse. Comparing preference of ankle–foot stiffness in below-knee amputees and prosthetists. *Scientific Reports*, 10, 2020. ISSN 20452322. doi: 10.1038/s41598-020-72131-2.

[11] Tyler R. Clites, Max K. Shepherd, Kimberly A. Ingraham, Les Wontorcik, and Elliott J. Rouse. Understanding patient preference in prosthetic ankle stiffness. *Journal of NeuroEngineering and Rehabilitation*, In Press(In Press):1–16, 2021. doi: 10.1186/s12984-021-00916-1.

[12] Billie J. Randolph, Leif M. Nelson, and M. Jason Highsmith. A review of unique considerations for female veterans with amputation. *Military medicine*, 18(Suppl. 4):66–68, 2016.

[13] United States Senate. Military Construction, Veterans Affairs, and Related Agencies Appropriations Act, 2017, 2016.

[14] Matthew J. Major, Andrew H. Hansen, and Elizabeth Russell Esposito. Focusing research efforts on the unique needs of women prosthesis users. *Journal of Prosthetics and Orthotics*, 2021. doi: doi:10.1097/JPO.0000000000000353.

[15] Matthew J. Major, Julia Quinlan, Andrew H. Hansen, and Elizabeth Russell Esposito. Effects of women's footwear on the mechanical function of heel-height accommodating prosthetic feet. *Plos One*, 17(1):e0262910, 2022. ISSN 19326203. doi: 10.1371/journal.pone.0262910. URL `http://dx.doi.org/10.1371/journal.pone.0262910`.

[16] Robert Gailey, Kerry Allen, Julie Castles, Jennifer Kucharik, and Mariah Roeder. Review of secondary physical conditions associated with lower-limb amputation and long-term prosthesis use. *Journal of Rehabilitation Research and Development*, 45(1):15–30, 2008. ISSN 07487711. doi: 10.1682/JRRD.2006.11.0147. URL `http://www.ncbi.nlm.nih.gov/pubmed/18566923`.

[17] Robert L. Waters and Sara Mulroy. The energy expenditure of normal and

pathologic gait. *Gait and Posture*, 9(3):207–231, 1999. ISSN 09666362. doi: 10.1016/S0966-6362(99)00009-0.

[18] Diana Zidarov, Bonnie Swaine, and Christiane Gauthier-Gagnon. Quality of Life of Persons With Lower-Limb Amputation During Rehabilitation and at 3-Month Follow-Up. *Archives of Physical Medicine and Rehabilitation*, 90(4):634–645, 2009. ISSN 00039993. doi: 10.1016/j.apmr.2008.11.003. URL http://dx.doi.org/10.1016/j.apmr.2008.11.003.

[19] Matthew J. Major and Nicholas P. Fey. Considering passive mechanical properties and patient user motor performance in lower limb prosthesis design optimization to enhance rehabilitation outcomes. *Physical Therapy Reviews*, 22(3-4):202–216, 2017. ISSN 1743288X. doi: 10.1080/10833196.2017.1346033. URL http://doi.org/10.1080/10833196.2017.1346033.

[20] Edward S Neumann. State-of-the-science review of transtibial prosthesis alignment perturbation. *Journal of Prosthetics and Orthotics*, 21(4):175–193, 2009.

[21] Fillauer. AllPro DM: Product Manual. URL https://fillauer.com/wp-content/uploads/2020/02/M065-AllPro-DM-Manual-10-21.pdf.

[22] Shane R. Wurdeman, Phillip M. Stevens, and James H. Campbell. Mobility Analysis of AmpuTees (MAAT I): Quality of life and satisfaction are strongly related to mobility for patients with a lower limb prosthesis. *Prosthetics and Orthotics International*, 42(5):498–503, 2018. ISSN 17461553. doi: 10.1177/0309364617736089.

[23] Brian J Hafner, Ignacio A Gaunaurd, Sara J Morgan, Dagmar Amtmann, Rana Salem, and Robert S Gailey. Construct Validity of the Prosthetic Limb Users Survey of Mobility (PLUS-M) in Adults With Lower Limb Amputation. In *Archives of Physical Medicine and Rehabilitation*, volume 98, pages 277–285, 2017. doi: 10.1016/j.apmr.2016.07.026. URL https://www.ncbi.nlm.nih.gov/pmc/articles/PMC5276724/pdf/nihms827934.pdf.

[24] Rajiv Singh, John Hunter, Alistair Philip, and Sarah Tyson. Gender differences in amputation outcome. *Disability and Rehabilitation*, 30(2):122–125, 2008. ISSN 09638288. doi: 10.1080/09638280701254095.

[25] Christopher M. Powers, Leslie Torburn, Jacquelin Perry, and Edmond Ayyappa. Influence of prosthetic foot design on sound limb loading in adults with unilateral below-knee amputations. *Archives of Physical Medicine and Rehabilitation*, 75 (7):825–829, 1994. ISSN 00039993. doi: 10.5555/uri:pii:0003999394901465. URL `https://www.archives-pmr.org/article/0003-9993(94)90146-5/pdf`.

[26] Edward D. Lemaire and F. Ronald Fisher. Osteoarthritis and elderly amputee gait. *Archives of Physical Medicine and Rehabilitation*, 75(10):1094–1099, 1994.

[27] Ezekiel J. Emanuel. The Real Cost of the US Health Care System. *JAMA*, 319 (10):983–985, 2018. ISSN 15339866. doi: 10.1097/01.ogx.0000544554.59124.26.

[28] Paul B. Ginsburg. High and rising health care costs: Demystifying U.S. health care spending. Technical report, Robert Wood Johnson Foundation, Princeton, NJ, 2008. URL `https://www.issuelab.org/resources/6461/6461.pdf`.

[29] OECD. Health at a Glance 2021: OECD Indicators, 2021. URL `https://www.oecd.org/health/health-at-a-glance.htm`.

[30] Roosa Tikkanen and Melinda K. Abrams. U.S. Health Care from a Global Perspective, 2019: Higher Spending, Worse Outcomes? Technical report, The Commonwealth Fund, 2019. URL `https://www.commonwealthfund.org/publications/issue-briefs/2020/jan/us-health-care-global-perspective-2019`.

[31] Michael Jason Highsmith, Jason T Kahle, Amanda L Lewandowski, Tyler D. Klenow, John J Orriola, Rebecca M Miro, Owen T. Hill, Silvia U. Raschke, Michael S. Orendurff, James T. Highsmith, and Bryce S. Sutton. Economic evaluations of interventions for transtibial amputees. *Technological Innovation*, 18(2-3):85–98, 2016. doi: doi:10.21300/18.2-3.2016.85.

[32] Phillip M. Stevens, John Rheinstein, and Shane R. Wurdeman. Prosthetic foot selection for individuals with lower-limb amputation: A clinical practice guideline. *Journal of Prosthetics and Orthotics*, 30(4):175–180, 2018. ISSN 10408800. doi: 10.1097/JPO.0000000000000181.

[33] Matthew J. Major, Martin Twiste, Laurence P.J. Kenney, and David Howard. Amputee Independent Prosthesis Properties-A new model for description and measurement. *Journal of Biomechanics*, 44(14):2572–2575, 2011. ISSN 00219290. doi: 10.1016/j.jbiomech.2011.07.016. URL `http://dx.doi.org/10.1016/j.jbiomech.2011.07.016`.

[34] United States Food and Drug Administration. Discussion Paper: 3D Printing Medical Devices at the Point of Care. Technical report, United States Food and Drug Administration, 2021.

[35] Mark A. Price, Philipp Beckerle, and Frank C. Sup. Design Optimization in Lower Limb Prostheses: A Review. *IEEE transactions on neural systems and rehabilitation engineering : a publication of the IEEE Engineering in Medicine and Biology Society*, 27(8):1574–1588, 2019. ISSN 15580210. doi: 10.1109/TNSRE.2019.2927094.

[36] Brian J. Hafner. Clinical prescription and use of prosthetic foot and ankle mechanisms: a review of the literature. *Journal of Prosthetics and Orthotics*, 17(4): S5–S11, 2005. ISSN 10408800. doi: 10.1097/00008526-200510001-00004.

[37] Brian J. Hafner, Joan E. Sanders, Joseph M. Czerniecki, and John Fergason. Energy storage and return prostheses: does subject perception correlate with biomechanical analysis? *Clinical Biomechanics*, 17:325–344, 2002.

[38] Brian J. South, Nicholas P. Fey, Gordon Bosker, and Richard R. Neptune. Manufacture of energy storage and return prosthetic feet using selective laser sintering. *Journal of Biomechanical Engineering*, 132(1):1–6, 1 2010. ISSN 01480731. doi: 10.1115/1.4000166. URL `http://biomechanical.asmedigitalcollection.asme.org/article.aspx?articleid=1428101%5Cn`.

[39] Nicholas P. Fey, Brian J. South, Carolyn C. Seepersad, and Richard R. Neptune. Topology Optimization and Freeform Framework for Developing Prosthetic Feet. In *International Solid Freeform Fabrication Symposium*, pages 607–619, 2009.

[40] Courtney E. Shell, Ava D. Segal, Glenn K. Klute, and Richard R. Neptune. The effects of prosthetic foot stiffness on transtibial amputee walking mechanics and balance control during turning. *Clinical Biomechanics*, 49(8):56–63, 2017. ISSN 18791271. doi: 10.1016/j.clinbiomech.2017.08.003. URL `http://dx.doi.org/10.1016/j.clinbiomech.2017.08.003`.

[41] Henry H. Warder, Joseph K. Fairley, Joshua Coutts, Richard R. Glisson, and Ken Gall. Examining the viability of carbon fiber reinforced three-dimensionally printed prosthetic feet created by composite filament fabrication. *Prosthetics and Orthotics International*, 42(6):644–651, 2018. ISSN 17461553. doi: 10.1177/0309364618785726.

[42] Zhen Tao, Hyoung-Jong Jong Ahn, Chenglong Lian, Kwang-Hee Hee Lee, and Chul-Hee Hee Lee. Design and optimization of prosthetic foot by using polylactic acid 3D printing. *Journal of Mechanical Science and Technology*, 31 (5):2393–2398, 2017. ISSN 1738494X. doi: 10.1007/s12206-017-0436-2. URL `www.springerlink.com/content/1738-494x`.

[43] Kathryn M. Olesnavage and Amos G. Winter. A Novel Framework for Quantitatively Connecting the Mechanical Design of Passive Prosthetic Feet to Lower Leg Trajectory. *IEEE Transactions on Neural Systems and Rehabilitation Engineering*, 26(8):1544–1555, 2018. ISSN 15344320. doi: 10.1109/TNSRE.2018.2848845.

[44] Kathryn M. Olesnavage, Victor Prost, William Brett Johnson, and V. G. Amos Winter. Passive prosthetic foot shape and size optimization using lower leg trajectory error. *Journal of Mechanical Design*, 140(10):1–11, 2018. ISSN 10500472. doi: 10.1115/1.4040779.

[45] Victor Prost, W. Brett Johnson, Jenny A. Kent, Matthew J. Major, and Amos G. Winter. Biomechanical evaluation over level ground walking of user-specific pros-

thetic feet designed using the lower leg trajectory error framework. *Scientific Reports*, 12(1):1–15, 2022. ISSN 20452322. doi: 10.1038/s41598-022-09114-y. URL `https://doi.org/10.1038/s41598-022-09114-y`.

[46] Victor Prost, W.B. Johnson, Jenny A. Kent, Matthew J. Major, and Amos G. Winter. Sensitivity investigation of the Lower Leg Trajectory Error framework and its implication for the design and evaluation of ankle-foot prostheses (in preparation), 2022.

[47] Victor Prost, Heidi V Peterson, and Amos G. Winter. Multi-keel passive prosthetic foot design optimization using the lower leg trajectory error framework. In *ASME 2021 International Design Engineering in Technical Conferences and Computers and Information in Engineering Conference*, pages 1–14, VIRTUAL, 2021.

[48] International Standards Organization. ISO 10328:2016 - Prosthetics — Structural testing of lower-limb prostheses — Requirements and test methods, 2016.

[49] W. Brett Johnson, Victor Prost, Pooja Mukul, and Amos G. Winter. Design and Evaluation of High-Performance, Low-Cost Prosthetic Feet for Developing Countries (in preparation), 2022.

[50] Victor Prost, Kathryn M. Olesnavage, W. Brett Johnson, Matthew J. Major, and Amos G. Winter. Design and testing of a prosthetic foot with interchangeable custom springs for evaluating lower leg trajectory error, an optimization metric for prosthetic feet. *Journal of Mechanisms and Robotics*, 10(2):1–8, 2018. ISSN 19424310. doi: 10.1115/1.4039342.

[51] Kathryn M. Olesnavage, Victor Prost, William Brett Johnson, Matthew J. Major, and Amos G. Winter. Experimental Demonstration of the Lower Leg Trajectory Error Framework Using Physiological Data as Inputs. *Journal of Biomechanical Engineering*, 143(3), 2021. ISSN 15288951. doi: 10.1115/1.4048643.

[52] Matthew J. Major, Joel Scham, and Michael Orendurff. The effects of common footwear on stance-phase mechanical properties of the prosthetic foot-shoe system. *Prosthetics and Orthotics International*, 42(2):198–207, 2018. ISSN 17461553. doi: 10.1177/0309364617706749.

Chapter 2

Stakeholder needs and design requirements

We identified key stakeholders and their needs through a combination of a review of technical literature and interactions with our research partner and funder, Hanger. Hanger is a leading provider of both patient care and product distribution in the prosthetics industry and is positioned to be a leader in providing amputee-specific, personalized prosthetic feet. By beginning to supply and distribute its own prosthetic feet, Hanger could expand on its existing roles in patient care and product distribution, thereby capturing additional revenue. Our work with Hanger included discussions with individuals from the business, clinical, and engineering divisions of the company as well as semi-structured interviews with Hanger prosthetists.

By understanding the flow of products, services, and capital between stakeholders in the clinical space (Fig. 2-1), we outlined design requirements for a personalized prosthetic foot which satisfies core requirements from each stakeholder. While these requirements are grounded in both literature and our interactions with Hanger, the literature is viewed within the context of the current product vision, where Hanger supplies, distributes, and provides the product.

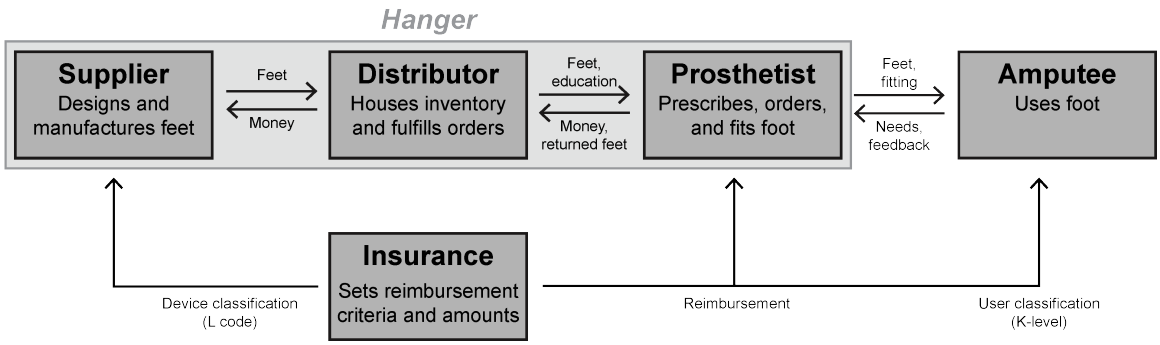

Figure 2-1: Diagram of the flow of products, services, and capital between stakeholders in the clinical space. The stakeholders (dark grey) interact with each other to exchange goods and value (arrows). In the envisioned product, Hanger (light grey) has a role in the supplier, distributor, and prosthetist segments by manufacturing, sourcing, and prescribing its own prosthetic feet.

2.1 Overview of key stakeholders

The primary stakeholders in the manufacturing and provision of a personalized prosthetic foot include suppliers, distributors, prosthetists, amputees, and insurance providers (Fig. 2-1). Prosthetics suppliers such as Ottobock, Össur, and Fillauer design and manufacture a variety of prosthetic components, including prosthetic feet. They sell these products, with a markup, to distributors such as Southern Prosthetic Supply (SPS), Hanger's distribution subsidiary and the largest distributor of prosthetic and orthotic components in the United States [1]. This markup cost generates profit for suppliers and covers operating expenses such as new product development and business overhead. Distributors house inventory from a vast array of suppliers and fulfill orders for specific products from clinics. SPS stocks more than 350,000 unique products, or stock-keeping units, from more than 750 suppliers [1]. In addition to selling devices, distributors often provide additional value to clinics by offering continuing education courses, which allow clinicians to maintain licensing status. A distributor's auxiliary role as an educator may enable it to further differentiate itself and improve engagement with clinicians [1].

Prosthetists and other clinical staff provide devices to amputee patients, interfacing with both distributors and insurance providers. They determine functional abilities and needs, select and fit appropriate prosthetic components, and work closely

with other members of a patient's clinical team, including physicians, occupational therapists, and physical therapists. In addition to ordering components from distributors, prosthetists sometimes return rejected prosthetic feet, which may happen if a patient has a brief trial period with multiple components [2, 3].

Amputee patients are the eventual end-users of prosthetic feet, and their preference is a significant indicator of prosthesis acceptance and commercial success [4]. Incorporating patient needs and values is not only good design practice, but it is also believed to improve quality of life and prosthesis acceptance [5]. Patient satisfaction is driven by prosthesis function [6–8] and appearance [6–9], which impact quality of life [9]. The Prosthesis Evaluation Questionnaire (PEQ) includes a specific Appearance Scale with questions about satisfaction with prosthesis appearance and the ability to wear shoes and different types of clothing [10]. There is some evidence that satisfaction with appearance is associated with overall device satisfaction [7], and many amputees desire a physiologically-realistic visual appearance of their prosthetic limb [6, 8].

Though amputees play a role in device selection, they do so in concert with their prosthetists, who play a significant role in translating patient needs to device selection and prescription. An individual's preference may not always match what is clinically appropriate, and patients sometimes present conflicting preferences; prosthetists help map patient needs and perceptions to appropriate prosthetic foot selection and alignment modifications [11, 12]. In this role, prosthetists act as curators, directing their patients to a small subset of appropriate potential prosthetic feet based on each user's specific needs. Prosthetic foot catalogs may contain several hundred prosthetic foot options [13–17]; rather than navigate the entire range of available products for each patient, many prosthetists will commonly prescribe from a much smaller range of products (~ 5) with which they have prior experience [2, 12]. These devices have demonstrated their economic value, durability, clinical performance, and patient acceptance. While prosthetics clinics may keep a small inventory of extra feet, these are typically previously worn, donated feet which are used for gait training or as a stop-gap measure if an amputee's foot breaks; in-clinic inventory does not provide a

sufficient selection to allow for trialing feet. Prosthetists must order individual prosthetic feet from distributors, and returning rejected feet is often not practical. As a result, most amputees only try on one foot [12] when selecting a new prosthetic foot.

All of the stakeholders are constrained by insurance requirements, which classify both prosthetic feet as well as amputee patients. In the United States, classification systems are governed by the Center for Medicare and Medicaid Services (CMS), but private insurance providers often choose to adopt the same coding and reimbursement mechanisms as federal providers. CMS classifies prosthetic feet according to L-codes, which are part of the Healthcare Common Procedure Coding System (HCPCS). This classification system uses alphanumeric codes to identify durable medical equipment, such as prosthetic feet, as well as other medical services and procedures. In this system, individual prosthetic foot models, such as the Fillauer All-Pro or the Freedom Highlander, are assigned a specific alphanumeric code, which designates a group of products performing similar functions and is associated with a specific insurance reimbursement amount. Amputees are grouped by the Medicare K levels, which define which types of prosthetic components are medically necessary for specific patients. Research-to-date has failed to connect medical condition, functional abilities, or outcome measures to K levels. CMS maintains that the K level system should not be seen as a functional classification of amputees, but rather that it should be considered a classification regarding the intended use of the device. K levels are commonly used in clinical practice, among other tools, to select appropriate components as they dictate the types of products for which a patient is eligible [18]. Though all prosthetists generate income for their clinics through insurance reimbursements for devices, clinics do not adopt the same philosophy toward distributor cost and reimbursement amount. Some clinics are driven by top-line revenue and focus on the total amount of sales, while others favor a bottom-line approach and fixate on net income and operating margins.

Historically, the requirements for prosthetic feet to receive specific L codes have been based on amputee-independent classification and testing. The American Orthotic and Prosthetic Association (AOPA), with input from foot manufacturers and

clinical researchers, created a set of standardized, mechanical tests for categorizing prosthetic feet [19]. These tests categorize prosthetic feet according to specific mechanical properties, such as their energy storage and return capabilities or axial torque absorption capabilities. The Pricing, Data Analysis and Coding (PDAC) contractor, the branch of CMS which assigns L codes, does not always accept the results of these mechanical tests as justification for specific L code. Nevertheless, the tests are considered to be industry-standard functional requirements, and insurance requirements provide a link between mechanical test standards and the reimbursement price and manufacturing cost for a design.

To be commercially successful, a new prosthetic foot must satisfy requirements from each stakeholder, but adoption will be driven by prosthetists. A new product must be providable through existing distribution and insurance mechanisms, or else it will not meet the desired market. This means it must meet the basic functional requirements for insurance reimbursement and satisfy the economic requirements of suppliers, distributors, and clinicians. The ultimate end-users, amputees, must like the device and feel that it meets their needs. Building trust in the clinical community through a straightforward customization process, proven durability, and enhanced walking performance for users will be necessary for breaking into this smaller subset of trusted, favorite devices. The commercial acceptance and success of a prosthetic foot is driven, in part, by prosthetist preference [4] and how frequently it is prescribed by prosthetists. A prosthetic foot which does not meet core functional requirements and which is not trusted by prosthetists is unlikely to be sold in the quantities necessary for commercial success.

2.2 Design requirements

We used our understanding of the customer value chain to define requirements, which center around the core value of creating a product line of personalized, high performance, and rapidly providable prosthetic feet. These design requirements are motivated by understanding the target user population, providing personalization in a

way that appeals to prosthetists, and satisfyiing insurance requirements. A full list of design requirements and specifications is enumerated in Table 2.1.

Table 2.1: Core design requirements for a high-performance, commercially viable, and personalized prosthetic foot

Requirement	**Measurable Parameter**
Customizable for patient at point-of-purchase	Heel height – 10 mm
	Foot size – size 18-30 cm
	User weight – 45-136 kg
	Build height – 140+ mm (with adaptor)
	Activity level – low/high options
Rapidly providable	Takes $\leq$ 2 business days from incoming order to outgoing shipment
High performance	Meets Freedom Highlander in subjective rating and clinical outcomes
Lightweight	Weighs $\leq$ 0.6 kg without cosmetic foot shell (in size 27 cm)
Passive	Does not use hydraulic or powered components
Compatible with L5981 standards	Passes ISO 10328/22675 tests
	Passes AOPA dynamic heel and keel tests
Compatible with US prostheses	Can be attached via standard pyramid adapter
	Is worn with existing commercial foot shell
Low-cost to manufacture	Manufacturing cost is below cost target (exact value is proprietary)

Personalization, or customization, is a core part of our value proposition for a new prosthetic foot. Some existing prosthetic feet provide a limited amount of post-purchase adjustability by mixing-and-matching reconfigurable modular components such as heel wedges or bumpers, and some prosthetists value this adjustability. This practice may stem from the limited resolution of existing size and stiffness options, and it may not reflect a desire or need for post-purchase adjustability of a personalized prosthetic foot. As a result, we focus on point-of-purchase customization, or personalization that happens when a prosthetist orders a device.

The foot size and user weight ranges are based both from existing commercial feet [13–17] and US population data [20]. The prosthetic foot is designed for K3 populations, which drives the heel height and build height requirements. To accommodate the heel rise in many shoes, cosmetic foot shells and the prosthetic feet that are worn within them have an elevated heel, which typically measures 10 mm (3/8") in K3 feet [13–17]. A prosthetic foot's build height involves a tradeoff: a lower build height (shorter foot) accommodates a greater range of residual limb lengths, but a taller build height allows the foot to store and return more energy. To balance this tradeoff, we selected a minimum build height of 140 mm, which is similar to the build height of the 6" (152 mm) Fillauer All Pro [13], a device which suppliers sometimes use as a benchmark for the height of new products.

Any adjustments a prosthetist can make in ordering a personalized prosthetic foot should be clinically meaningful. The LLTE design framework could allow clinicians to fine tune the "activity level" of a patient by specifying the walking activities for which the foot is designed, such as walking up ramps or walking quickly on flat ground [21, 22]. Although we have the capability to quantitatively design a prosthetic foot for a specific activity, an infinite resolution of activity level options is likely unnecessary. Beyond a certain granularity, adjustments to the target user profile may be neither repeatable nor clinically meaningful.

To operate within existing prosthetist workflows, another key value is rapid provision. The required fulfillment time of less than two business days from order receipt is based off of the lead time from order receipt to shipment of current products [1]. While prosthetists may be willing to accept a slightly longer lead time in exchange for a higher degree of amputee-specific personalization, increasing the fulfillment time beyond two days may create a barrier to adoption by disrupting prosthetist workflows and potentially straining clinics' cash flows and finances [23], and create a barrier to adoption.

For prosthetists to change their existing behaviors and prescribe a new prosthetic foot, the new product would need equivalent or better performance than existing products. We selected the Freedom Highlander as a commercial benchmark due to

its widespread acceptance and provision in the clinical community.

This prosthetic foot is designed for distribution in the US under L5981, a category of ESR prosthetic feet commonly prescribed to K3/4 amputees. Traditionally, passing the AOPA dynamic heel and keel tests has been considered criteria for classification as an L5981 product. To pass these tests, a prosthetic foot must exceed a given amount of deformation and energy return efficiency in representative heel and keel loading scenarios [19]. To demonstrate strength and durability, particularly for insurance providers, prosthetic feet must also survive both static and cyclic load testing according to ISO 10328 [24] or 22675 [25]. Satisfying the ISO strength and durability tests requires that a prosthetic foot be strong enough to withstand both high single-cycle loads (static proof and ultimate strength) and lower magnitude multi-cycle loads (fatigue) without plastic deformation [24].

Compatibility with the common ESR prosthetic attachment systems and form factors in the US is necessary for adoption by prosthetists and acceptance by amputee patients. To best utilize prosthetists' clinical experience and avoid retraining with an additional mounting system, a personalized prosthetic foot must attach to the rest of the prosthesis using a standard pyramid adapter. Many amputees desire a physiological prosthetic foot appearance [6, 8]; to achieve this appearance with the walking performance provided by existing ESR feet, L5981 feet are commonly worn within a commercial foot shell, which is a thin, removable foam enclosure which looks like a physiological foot and houses the prosthetic foot. Rather than design a new foot shell for our prosthetic foot, we require that the foot fit within an existing shell.

Our prosthetic foot is also designed to be low-cost to manufacture. To meet this need, we set an upper cost threshold relative to the minimum reimbursement for the L5981 code. Reimbursement amounts vary geographically across the United States and fluctuate over time. In October 2021, the minimum non-rural reimbursement for L5981 devices was $2994.97 [26]. The specific cost threshold cannot be disclosed for proprietary reasons, but the target is set to be compelling to the supplier-distributor as well as prosthetists. While a lower cost to manufacture than existing ESR feet does not reduce insurance reimbursement prices, it positions the supplier-distributor and

prosthetists to operate with strong bottom-line revenue and high profit margins, even if insurance reimbursements decrease relative to inflation. Though many prosthetists commonly utilize a subset of trusted prosthetic feet [2, 12], good clinical performance, durability and increased revenue to clinic increase the likelihood of them prescribing a new product.

Bibliography

[1] Hanger Inc. Investor Presentation, 2022.

[2] Gerald Stark. Perspectives on how and why feet are prescribed. *Journal of Prosthetics and Orthotics*, 17(4 SUPPL.):18–22, 2005. ISSN 10408800. doi: 10.1097/00008526-200510001-00007.

[3] Elisabeth Schaffalitzky, Pamela Gallagher, Malcolm MacLachlan, and Stephen T. Wegener. Developing consensus on important factors associated with lower limb prosthetic prescription and use. *Disability and Rehabilitation*, 34(24):2085–2094, 2012. ISSN 09638288. doi: 10.3109/09638288.2012.671885.

[4] Brian J. Hafner, Joan E. Sanders, Joseph M. Czerniecki, and John Fergason. Energy storage and return prostheses: does subject perception correlate with biomechanical analysis? *Clinical Biomechanics*, 17:325–344, 2002.

[5] Elisabeth Schaffalitzky, Sinead Ni Mhurchadha, Pamela Gallagher, Susan Hofkamp, Malcolm MacLachlan, and Stephen T. Wegener. Identifying the values and preferences of prosthetic users: A case study series using the repertory grid technique. *Prosthetics and Orthotics International*, 33(2):157–166, 2009. ISSN 03093646. doi: 10.1080/03093640902855571.

[6] Erwin C. Baars, Ernst Schrier, Pieter U. DIjkstra, and Jan H.B. Geertzen. Prosthesis satisfaction in lower limb amputees: A systematic review of associated factors and questionnaires. *Medicine*, 97(39), 2018. ISSN 15365964. doi: 10.1097/MD.0000000000012296.

[7] Sophie Ritchie, Sally Wiggins, and Alison Sanford. Perceptions of cosmesis and function in adults with upper limb prostheses: A systematic literature review. *Prosthetics and Orthotics International*, 35(4):332–341, 2011. ISSN 03093646. doi: 10.1177/0309364611420326.

[8] Robin Bekrater-Bodmann. Factors Associated With Prosthesis Embodiment and

Its Importance for Prosthetic Satisfaction in Lower Limb Amputees. *Frontiers in Neurorobotics*, 14, 2021. ISSN 16625218. doi: 10.3389/fnbot.2020.604376.

[9] Neil Harness and Michael Pinzur. Health related quality of life in patients with dysvascular transtibial amputation. *Clinical Orthopaedics and Related Research*, 383:204–207, 2001.

[10] Marcia W. Legro, Gayle D. Reiber, Douglas G. Smith, Michael Del Aguila, Jerrie Larsen, and David Boone. Prosthesis evaluation questionnaire for persons with lower limb amputations: Assessing prosthesis-related quality of life. *Archives of Physical Medicine and Rehabilitation*, 79(8):931–938, 1998. ISSN 00039993. doi: 10.1016/S0003-9993(98)90090-9.

[11] Niels Jonkergouw, Maarten R. Prins, Arjan W.P. Buis, and Peter Van Der Wurff. The effect of alignment changes on unilateral transtibial amputee's gait: A systematic review. *PLoS ONE*, 11(12):1–18, 2016. ISSN 19326203. doi: 10.1371/journal.pone.0167466.

[12] Max K. Shepherd and Elliott J. Rouse. Comparing preference of ankle–foot stiffness in below-knee amputees and prosthetists. *Scientific Reports*, 10, 2020. ISSN 20452322. doi: 10.1038/s41598-020-72131-2.

[13] Fillauer. Lower Extremity Prosthetics Product Catalog, 2020. URL `fillauer.com`.

[14] Endolite North America. Catalog 2016/2017 - Lower limb prosthetic product range, 2016.

[15] Freedom Innovations. Lower Limb Prosthetic Solutions Product Catalog, 2015.

[16] Ottobock. Prosthetics - Lower limbs, 2015.

[17] Össur. Prosthetic Solutions Catalogue, 2016.

[18] Dylan Borrenpohl, Brian Kaluf, and Matthew J. Major. Survey of U.S. Practitioners on the Validity of the Medicare Functional Classification Level System and Utility of Clinical Outcome Measures for Aiding K-Level Assignment. *Archives of Physical Medicine and Rehabilitation*, 97(7):1053–1063, 2016. ISSN 1532821X. doi: 10.1016/j.apmr.2016.02.024. URL http://dx.doi.org/10.1016/j.apmr.2016.02.024.

[19] American Orthotic and Prosthetic Association. AOPA Prosthetic Foot Project Report. Technical report, American Orthotic and Prosthetic Association, 2010.

[20] Centers for Disease Control and National Center for Health Statistics. National Health and Nutrition Examination Survey Data, 0.

[21] Victor Prost, Heidi V Peterson, and Amos G. Winter. Multi-keel passive prosthetic foot design optimization using the lower leg trajectory error framework. In *ASME 2021 International Design Engineering in Technical Conferences and Computers and Information in Engineering Conference*, pages 1–14, VIRTUAL, 2021.

[22] Victor Prost. *Development and Validation of a Passive Prosthetic Foot Design Framework based on Lower Leg Dynamics*. PhD thesis, Massachusetts Institute of Technology, 2021.

[23] Gary M Berke and Brenda L Berke. The Impact of Delivery Delays in Prosthetic Care. *The O&P Edge*, 5 2022. URL https://opedge.com/the-impact-of-delivery-delays-in-prosthetic-care/.

[24] International Standards Organization. ISO 10328:2016 - Prosthetics — Structural testing of lower-limb prostheses — Requirements and test methods, 2016.

[25] International Standards Organization. ISO 22675:2016 Prosthetics — Testing of ankle-foot devices and foot units — Requirements and test methods, 2016. URL https://www.iso.org/standard/70203.html.

[26] Centers for Medicare & Medicaid Services. October 2021 DMEPOS Fee Schedule Update, 2021.

Chapter 3

Material and manufacturing process selection

3.1 Candidate materials

ESR prosthetic feet are able to store and return energy with each step, and they are strong enough to withstand years of daily use. Instead of focusing on individual material properties such as elastic modulus, yield strength, or ultimate strength, we utilized material performance indices [1] which directly relate to the energy storage and strength requirements of the ISO and AOPA tests (Sec. 2.2, Table 2.1).

The ability of a prosthetic foot to satisfy these requirements relates to both its material and geometry. In this work, we quantify material performance through two performance indices, the strain energy density and the relative strength factor (Fig. 3-1), which quantify the material's energy storage and strength capabilities. High performing materials on both indices also result in high performing (low LLTE) prosthetic feet (Sec. 3.4.1); the first-order indices in this section allow for rapid evaluation of many materials instead of performing a foot design optimization for each material candidate.

Material properties are compared to Nylon 6/6 (Fig. 3-1), a high performance and relatively inexpensive thermoplastic which we have used extensively in prior work [2–7]. Values for both performance indices are divided by the values for Nylon 6/6.

High scores correspond to high performing materials, with values greater than one indicating that a material outperforms Nylon 6/6 (tensile modulus $E = 2.49$ GPa, tensile yield stress $\sigma_y = 73.7$ MPa, poisson ratio $\nu = 0.6$, and density $\rho = 1130$ kg/m^3).

Properties are given from manufacturer-supplied tensile data [8–16] or tensile data in academic publications [17–19]. Although bending is the primary deformation mechanism in ESR prosthetic feet, flexural data is less commonly available, and material properties for tensile and flexural testing are well-correlated for the polymers and composites considered here [1]. A variety of additive manufacturing (AM) processes are evaluated: fused filament fabrication (FFF) from Markforged, Stratasys, and other companies; the related fiber-reinforced continuous fiber fabrication (CFF) process from Markforged; HP Multijet Fusion and other powder bed fusion (PBF) processes; and other processes such as stereolithography (SLA) and digital light synthesis (DLS). Conventional material production methods such as casting and extrusion are also included.

The first performance index, the strain energy density represents a material's potential for recoverable energy storage. The strain energy density u_{SE} for a material with elastic modulus E, yield stress σ_y, and yield strain ϵ_y is given as:

$$u_{\text{SE}} = \sigma_y \epsilon_y = \frac{\sigma_y^2}{E}, \tag{3.1}$$

with units of energy per unit volume [J/m^3]. A material with a high strain energy density is able to store a large amount of energy per unit volume before reaching the yield stress. For materials which fail by brittle fracture instead of plastic yield, σ_y and ϵ_y can be replaced with fracture stress σ_f and strain ϵ_f, respectively. A material with a normalized score greater than one (Fig. 3-1) can elastically store and return more energy per unit volume than Nylon 6/6.

While the strain energy density metric quantifies material performance, it does not consider the base geometry which will be used. The relative strength factor quantifies both material and geometric performance; it represents how much a design

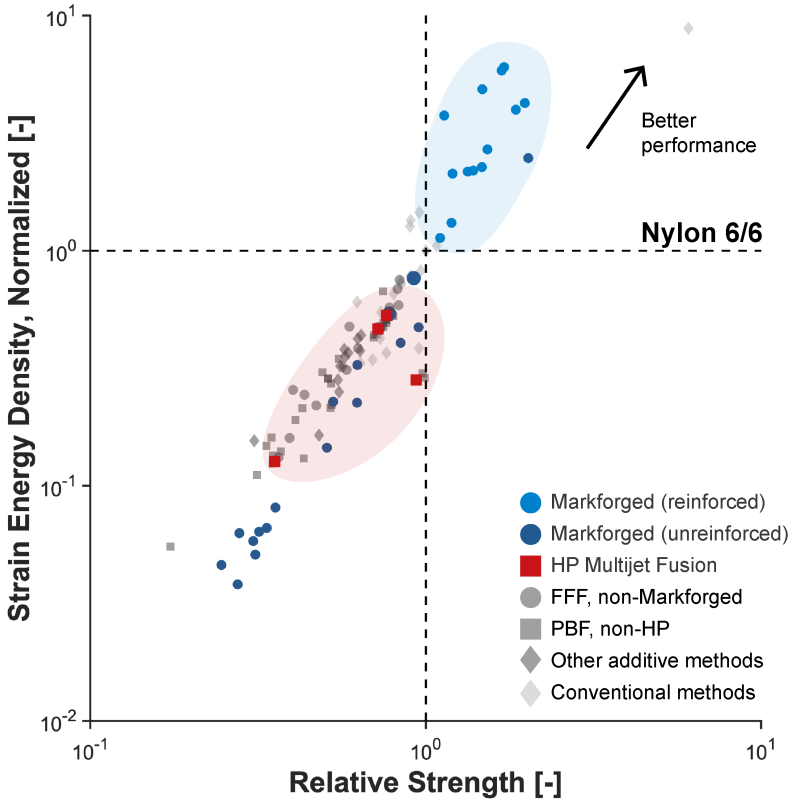

Figure 3-1: Ashby-style plot representing the two primary material selection indices used in this work: the strain energy density and the relative strength factor metric. All data are normalized to the properties of Nylon 6/6; values ≥ 1 represent higher performance than Nylon 6/6.

must change to meet safety factor constraints. A material and design with a low relative strength factor will be less strong than one with a high score; it is not possible for the weaker material to sustain the same loads with the same bending stiffness. To satisfy the strength (load) requirement, the weaker material requires a stiffer design. While this reduces the maximum strain on the design, it also forces it to be stiffer than it optimally would be.

The relative strength factor is calculated by comparing the strength of two cantilevered beams with the same equivalent bending stiffness, $(EI)_{\text{eff}}$, but different materials and cross-section geometries:

$$(EI)_{\text{eff}} = (EI)_i = \frac{1}{12} E_i w_i t_i^3, \tag{3.2}$$

where E_i and I_i represent the elastic modulus and second moment of area for beam i with width w_i and thickness t_i. Solving Eqn. 3.2 for t_i in terms of $(EI)_{\text{eff}}$ gives

$$t_i = \left(\frac{12(EI)_{\text{eff}}}{w_i E_i} \right)^{1/3}. \tag{3.3}$$

To maintain the same effective bending stiffness, a beam of a softer material (lower E_i) must be thicker (higher t_i), if both beams have the same width w. The maximum stress and safety factor associated with a tip loaded, cantilever beam-based design is given as:

$$\sigma_{\max} = \frac{FLy_{\max}}{EI} = \frac{FL}{(EI)_{\text{eff}}} \left(\frac{t_i}{2} \right) \propto E_i^{2/3}. \tag{3.4}$$

Comparing the maximum stress associated with loading a design (Eqn. 3.4) to its yield strength gives a safety factor SF and relative strength factor γ_{SF}:

$$SF = \frac{\sigma_y}{\sigma_{\max}} \propto \frac{\sigma_y}{E_i^{2/3}} \tag{3.5}$$

$$\gamma_{\text{SF}} = \frac{\sigma_y}{E_i^{2/3}}. \tag{3.6}$$

This analysis considers cantilever beams with a solid cross section ($I = \frac{1}{12} w t^3$),

but the relative strength factor calculations can be extended to beams with more complex cross sections such as leaf springs, I-beams, or multi-material, composite beams. A combination of material and geometry with a normalized relative strength score below one is weaker than Nylon 6/6. This means we must add material to meet the same stress or safety factor constraints, resulting in a stiffer prosthetic foot and decreased walking performance (increases LLTE).

Extruded Nylon 6/6 outperforms additively manufactured (AM) polymer materials (Fig. 3-1). Among these polymers, the Nylon 11- and 12-based materials from HP are the highest performing. Of all AM materials considered, only the Nylon-reinforced composites from Markforged could potentially outperform extruded Nylon 6/6; however, their behavior is more uncertain due to a lack of consensus on how the location and quantity of fiber reinforcement impacts stiffness and part failure [20–24], limited research of the fatigue behavior of printed composites [25, 26], and significant part-to-part variability in mechanical properties [27]. Cast urethanes offer similar performance to extruded Nylon 6/6, but casting has a limited ability to accommodate the geometric features needed for a commercially-appropriate prosthetic foot form factor. Additionally, casting requires fixed tooling, which is not appropriate for manufacturing a personalized product at scale. Comparing materials based on performance metrics revealed three primary candidates: extruded, machined Nylon 6/6; Nylon-based composites from Markforged; and Nylon 11 and 12 from HP.

3.2 Manufacturing rate, cost, and quality

3.2.1 Rate comparison

The manufacturing rate, or the speed at which parts can be produced, directly connects to our design requirements (Table 2.1) and impacts the overall manufacturing cost. A manufacturing process which takes more than two business days to produce an individual prosthetic foot does not satisfy this requirement and is not viable. Compared with a faster and higher throughput process, a slower manufacturing rate

requires purchasing additional equipment to meet the same production volume.

The overall manufacturing time was estimated using a representative early-stage model of the prosthetic foot design for three processes: CNC machining of Nylon 6/6, Markforged's continuous filament fabrication, and HP's multijet fusion. CNC machining time was estimated using a material removal rate calculation. A material removal rate MRR of 26 cm^3/min, and a total volume of material V_t of 1200 cm^3 gives an estimated machining time $t = \frac{V_t}{MRR} = 46$ minutes, or 0.77 hr/foot. For a single prosthetic foot with a base material of Nylon White (solid infill) reinforced with Kevlar (two concentric fiber rings, 150 reinforced layers), Markforged's Eiger software predicted a print time of 48 hours on either its desktop or industrial machines. For a fully nested build of 25 parts with same part file and a base material of Nylon 12, HP's SmartStream software predicted a build time of eight hours and cooling time of eight hours, for a total of 16 hours, giving an average of 0.64 hr/foot. Both HP MJF and CNC machining can satisfy the ≤ 2 business day time requirement to design and manufacture a prosthetic foot (Table 2.1), but Markforged does not meet this requirement.

3.2.2 Cost comparison

This cost analysis focuses on well-structured, engineering-specific costs of manufacturing [28] from materials, equipment, and overhead, which are the focus of many existing cost models [29–35]. We use parametric models to represent the individual cost contributions from materials, equipment, and overhead; these can be modeled for a variety of manufacturing processes, including subtractive processes like machining [36] and additive processes [29–32, 35, 37].

Engineering-specific manufacturing costs are only one aspect of the overall cost produce and distribute a personalized prosthetic foot; the overall cost to a supplier-distributor will be significantly greater than the manufacturing cost alone. Focusing on manufacturing cost neglects other costs which contribute to production cost. These costs may result from factors such as leasing or ownership of a manufacturing facility, inventory and transportation, supply chain management, and vulnerability to supply

chain disruption, and they are often considered ill-structured [28]. These costs depend less on the manufacturing process selected and more on how the specifics of how the process is implemented; as a result, they are more difficult and subjective to estimate, particularly during early-stage product development [28]. The goal of the parametric cost model is not to provide exact cost predictions. Instead, this analysis aims to provide intuitive and interpretable first-order insights about cost tradeoffs [33], facilitating process-to-process comparisons and guiding early-stage process decisions.

The overall per-part manufacturing cost C_{total} represents the anticipated cost to manufacture an individual prosthetic foot. This consists of the material cost C_{mat} of the raw materials used, the equipment cost C_{eq} to purchase and maintain the machines, and the overhead cost C_{overhead}, which includes costs of operator time to set up and post-process a part as well as the cost of energy to run the machines:

$$C_{\text{total}} = C_{\text{mat}} + C_{\text{eq}} + C_{\text{overhead}} \tag{3.7}$$

In addition to using the lower-level relationships between anticipated production volume and production costs from prior work [29–32], we included additional variables to capture relevant behaviors for this production scheme. The fail fraction α_{fail} represents a fraction of failed parts. For some additive manufacturing processes, this value may be as high as 10% due to dislocation errors or part warping, but it may be as low as 1% for machining due to better machine and process control. Failed parts increase the overall material usage, number of machines required, energy costs, and operator costs to produce the same number of output parts; including this cost in the model provides a more fair comparison of processes with different failure or yield rates. The surge fraction α_{surge} represents the anticipated variation in average weekly production rate. High week-to-week variation in demand with the same number of machines results in overly long lead times when demand increases. Increasing the number of machines can allow a manufacturer to meet the desired lead time requirements despite increases in demand, but additional machines also incurs additional cost. Including this parameter provides insight into how much costs is

added to maintain the same production rate despite increases in demand. Lastly, the number of desired production facilities $n_{\text{facilities}}$ represents the number of individual production facilities. In this analysis, we assume demand is distributed evenly among each facility, but that does not have to be the case.

General production parameters include the target production volume [parts/year], the part volume [cm^3/part], the number of production facilities $n_{\text{facilities}}$, energy price [USD/kWh], operator salary [USD/hour], operator attendance fraction, load factor, and the surge fraction. Process-specific parameters include part failure fraction, machine replacement fraction, parts per print, manufacturing time, material cost, scrap fraction, machine cost, machine maintenance cost, setup time, post-processing cost, and machine power. Three process-material combinations were modeled: composite Markforged (Markforged CFF), plastic HP Multijet Fusion (HP MJF), and CNC machining of Nylon 6/6. Key governing equations and input parameter values are described in more detail in Sec. 3.4.3.

All cost predictions demonstrate similar characteristic features (Fig. 3-2). As production volume increases, equipment costs generally decrease, but they show spikes due to incremental machine purchases. As production volume increases, the spikes decay in magnitude, and the equipment cost approaches full utilization of the machine. Material costs are fixed across production volumes. If there is an economy of scale for purchasing these raw material, it is generally small, and information about the magnitude of this cost savings is not publicly available. As a result, this trend is not included in the cost model, and material costs are fixed across production volumes. By assuming that all designs are unique, overhead costs are fixed across manufacturing scales; each part requires the same amount of operator setup time and energy usage, regardless of the yearly production volume.

In each process, cost is driven by a different component. Expensive material costs for composite materials contribute a significant portion of the overall cost for the Markforged CFF process. The HP MJF process is fast (if fully utilized, approximately 45 minutes per foot), but machines are expensive; at low production volumes, the high machine cost dominates. Machining costs are dominated by overhead costs, which

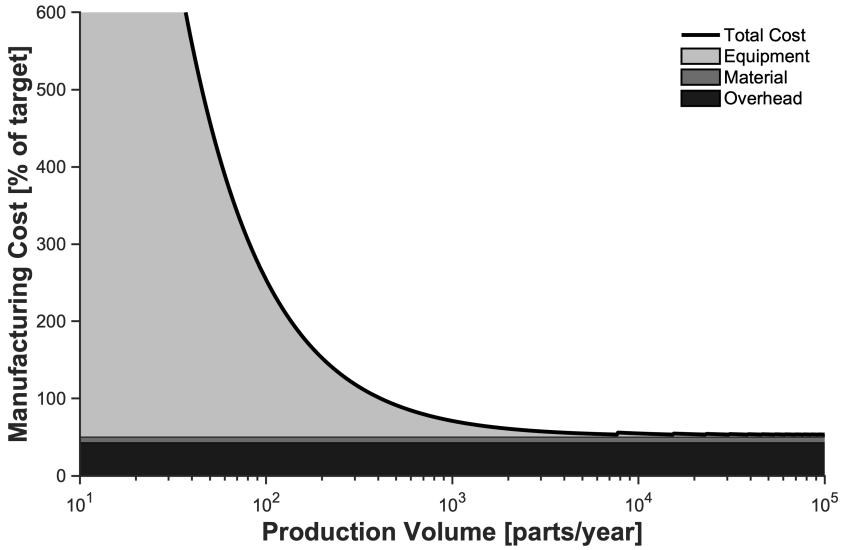

Figure 3-2: Anticipated manufacturing cost vs. production volume for CNC machining of Nylon 6/6. Costs are shown as a percentage of the target manufacturing cost. Data are shown for a representative combination of model inputs, and costs are separated by component. Equipment costs (light grey) generally decrease with increasing production volume but show decaying spikes due to incremental machine purchases. At scale, the cost of CNC machining is driven by overhead costs due to energy and operator salaries.

includes the operator time to both set up the workpiece and to create the machining toolpaths. At scale, this process can likely be partially or fully automated using commercially-available computer-aided manufacturing (CAM) automation software. At production volumes above 1000 parts/year, costs are similar for HP MJF and CNC machining (Fig. 3-3). Costs for both processes satisfy the functional requiremen. The Markforged CFF process will likely cost about twice as much, which exceeds the functional requirement.

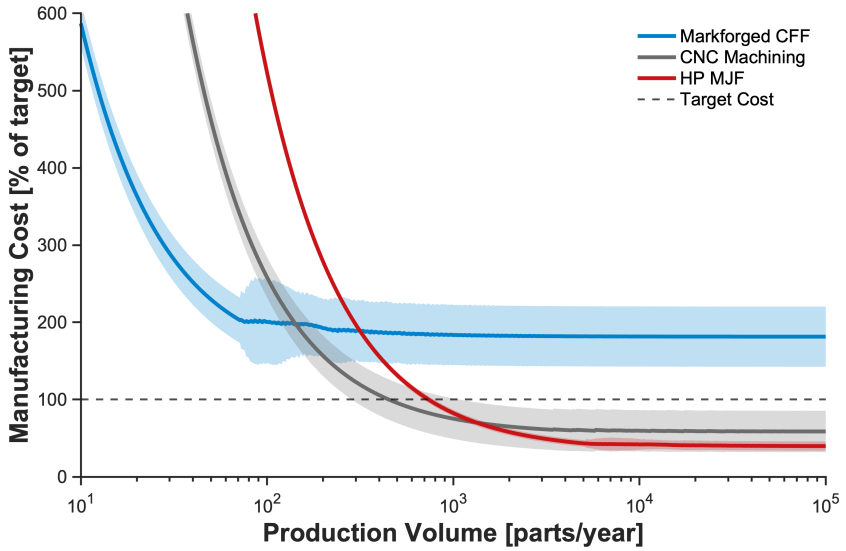

Figure 3-3: Cost comparison of different manufacturing processes across a range of production volumes. Average costs for Markforged CFF (blue), HP MJF (red), and CNC machining (dark grey) are represented by solid lines, with the minimum and maximum predicted costs represented by shaded bands. Costs are normalized by the target manufacturing cost, shown by the horizontal grey line.

3.2.3 Quality comparison

Manufacturing quality can be described in many ways, from performance- and durability-related metrics to factors such as reliability, aesthetics, and perceived quality [38]. We have previously considered material performance and durability as overall quality indicators in Sec. 3.1. Here, we focus on process reliability. Creating high resolution and personalized prosthetic feet centers on the value proposition that user-specific designs could be superior to existing ESR feet, which are available in a low resolution

of size and stiffness categories. A high variability manufacturing process may not provide this value, as it will not consistently result in prosthetic feet with the target static or fatigue behavior.

The outputs of all manufacturing processes are subject to variability, which might be due to variations in the raw material or inconsistent machine behaviors. This results in variations in part stiffness due to changes in material properties and manufactured part geometry, which can be modeled by representing the prosthetic foot structure as an Euler Bernoulli beam. A beam with Young's Modulus E, moment of inertia I, and length L has an effective bending stiffness $k = \frac{3EI}{L^3}$, or $k \propto EI$. Variation in stiffness is directly proportional to variation in Young's Modulus (material) and variations in moment of inertia (geometry).

A 5% change in modulus results in a 5% change in stiffness. Variation in part-to-part elastic modulus may depend on the process parameters and part configuration. For Markforged CFF, one study reports part-to-part variation of flexural modulus of 3.5%-7.9% [17], while another reports variation ranging from 1.6% to 22.2% [24]. For HP MJF, this variation has been reported as 0.7% to 4.5%, depending on the part orientation [39]. The variation in extruded Nylon 6/6 is 1.2% [19], which is similar or better than HP, and lower than the variation in Markforged CFF material properties. The part-to-part variation of Markforged CFF parts exceeds the amputee-perceivable difference in stiffness [40].

While geometric repeatability is generally good for Markforged CFF, HP MJF, and CNC machining, these tolerances can become significant for the part geometries considered in this work. Thermal strain during part cooling [41] in both the CFF and MJF processes can lead to thermal distortion, which manifests as part contraction and warping. While this effect is small for relatively thin and small parts, such as those used for the materials tests common in literature, thermal strain is much greater for thick, large parts such as the prosthetic foot geometries considered. Dimensional tolerance in CNC machining is often specified to ISO 2768 medium tolerance [42], which provides a maximum permissible deviation based on the nominal part dimension, such as ± 0.2 mm for dimensions between 6 mm and 30 mm. This

corresponds to an overall change in stiffness ranging from 0.2/30 mm/mm to 0.2/60 mm/mm, or 0.7%-3.3% change in stiffness due to geometric variation, which is below the amputee-perceivable difference in stiffness [40].

3.3 Justification of chosen material and manufacturing process

With current manufacturing capabilities, CNC machining of Nylon 6/6 is the process-material combination which best satisfies the core design requirements (Table 2.1). Nylon 6/6 is a high-performance material which can elastically store and return large amounts of energy during the stance phase of walking, and CNC machining is the process which best satisfies manufacturing rate, cost, and quality requirements. Although additive manufacturing is often seen as the hallmark process for customized products, current commercially-available materials and processes do not match the material performance, manufacturing rate, cost, and quality of CNC machining of Nylon 6/6. While Markforged composites could potentially provide higher material performance, the process does not meet requirements for manufacturing rate, cost, or quality. HP's Nylon 11- and 12- based materials do not perform well enough in a prosthetic foot, but the process satisfies rate, cost, and quality requirements. Nylon 6/6 is a high-performance material, and CNC machining can satisfy rate, cost, and quality requirements, even when prosthetic feet are machined as one-of-a-kind, unique parts.

3.4 Supplementary information

3.4.1 Relationship between material performance indices and LLTE

To confirm that the material performance indices in Sec. 3.1 provide a reasonable prediction of a material's suitability for creating ESR prosthetic feet, the single-keel

foot architecture used in [3, 4] was optimized for a variety of AM materials for an example user (Table 3.1).

Table 3.1: Optimization setup parameters

Parameter	Value
User mass [kg]	57
Lower leg length [m]	0.485
Foot size [cm]	26
Ankle height [m]	0.115
Fillet radius [m]	0.005
Walking activity [–]	Flat ground walking
Safety factor [–]	2

As anticipated, materials with strain energy density and relative strength factors result in prosthetic feet with better walking performance, as quantified through lower LLTE scores (Fig. 3-4). This confirms that these performance indices are useful, quick-to-compute indications of a material's suitability; each point on the graph in Fig. 3-4 is the result of ~ 10 hours of optimization, but computing relative strength and strain energy density is instantaneous.

Above a certain level of material performance, geometry becomes the limiting factor for foot performance; increasing the relative strength or strain energy density further provides minimal, if any, improvement to LLTE. For the optimization results presented here, this occurs at relatively small strain energy density and relative strength values; however, the exact location of this plateau may not generalize to other foot geometries or loading scenarios. A commercial prosthetic foot must be designed to pass ISO 10328 ultimate strength and fatigue tests, not only to survive a user walking on flat ground. The maximum ISO loads are about three to five times user body weight [43], greater than the safety factor used in this optimization experiment. Feet designed to survive greater loads may exhibit a plateau at higher relative strengths or strain energy densities than the feet presented here.

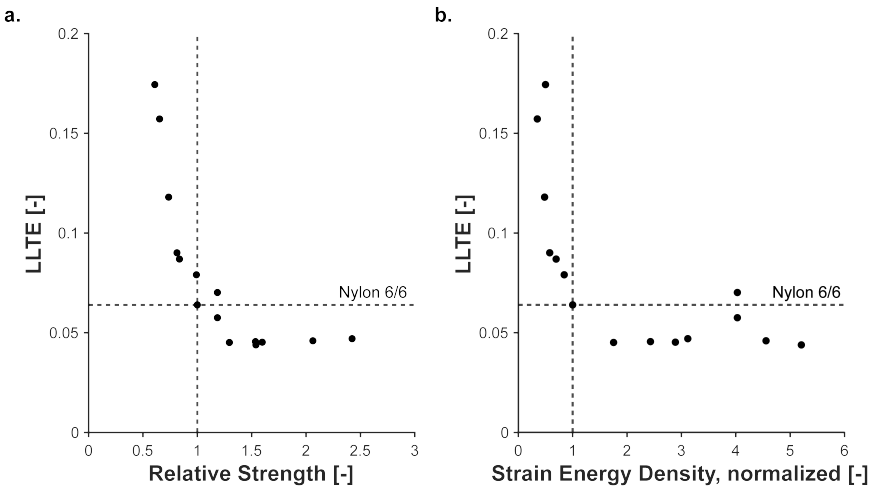

Figure 3-4: LLTE scores and material performance indices for example materials. Prosthetic foot designs were optimized for a representative user with a variety of reference materials. High values of both relative strength (a) and strain energy density (b) were associated with improved walking performance (lower LLTE).

3.4.2 Relative strength of more complex cross sections

Sec. 3.1 introduced the concept of relative strength as material performance index to compare both the viability of a material and of a geometry for creating high performance ESR prosthetic feet; however, the previous sections focused on comparing various materials for a single geometry, a simple cantilever beam with uniform, solid cross section. This approach quantifies how material selection impacts performance for one geometry, but it does not demonstrate the utility of the relative strength factor for comparing more complex or multi-material structures. In practice, a higher performing geometry made from a lower performance material may enable similar relative strength as the solid cross section made of Nylon 6/6. In this section, we demonstrate the use of the relative strength to compare other cross sections: multi-material models (Fig. 3-9) and split, double, and triple keel geometries (Fig. 3-5).

Laminated multi-material structures (Fig. 3-5 often fail at their outer faces. These faces are the locations of highest strain, but the composite materials often used for these features show failure at relatively small strains. A cross section geometry which brings material closer to the neutral axis could provide relatively greater performance than the original solid geometry. The relative performance improvement achieved by

changing cross section is also expected to be greater (though slightly) for a laminated composite beam than for a uniform material section.

The laminated multi-material representation also has a physical basis in the Markforged CFF process. Based on the size of prosthetic feet and the anisotropy of CFF, the best print orientation involves manufacturing layers parallel to the sagittal plane (Fig. 3-6. Fiber placement is driven by the Markforged CFF process requirements, which only place fiber concentrically along a part's edges. Although CFF also allows for raster-based "isotropic" fiber reinforcement, this reinforcement method is associated with part failure at lower strains than those found for concentric reinforcement.

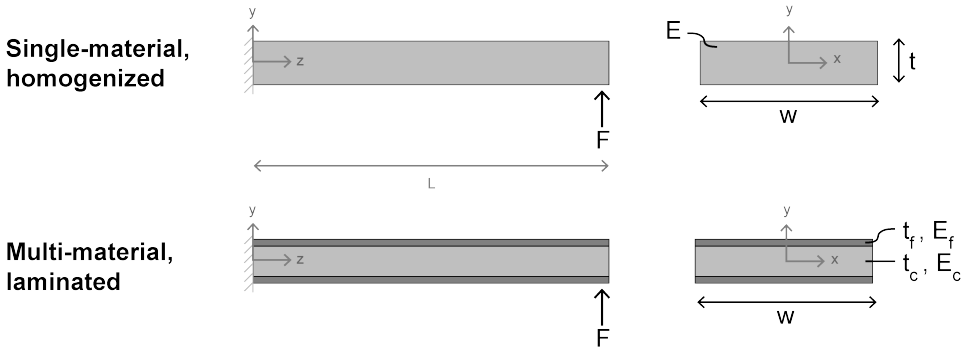

Figure 3-5: Diagram of single- and multi-material cross sections. A multi-material beam is made of two materials: an inner, softer core and the outer, stiffer fiber plate.

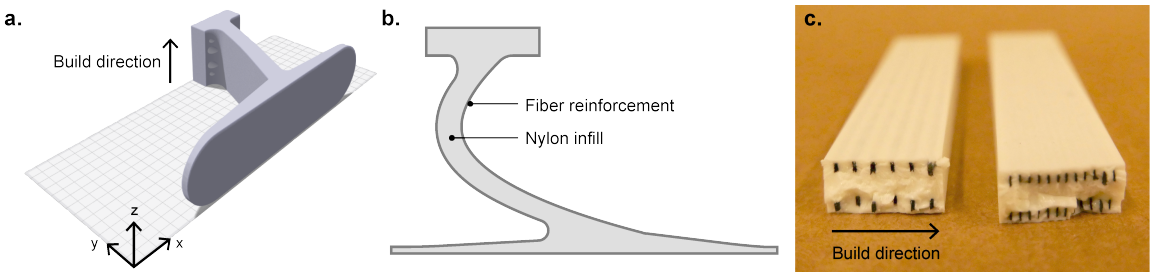

Figure 3-6: Overview of Markforged CFF process. a) Diagram of prosthetic foot geometry within the Mark Two's build volume, with the build volume and layers parallel to the sagittal plane of the foot. b) Diagram of concentric fiber reinforcement strategy, in which a band of stiff fiber surrounds a Nylon infill. c) Photograph of two fractured Markforged CFF specimens with different numbers of fiber layers.

A laminated cantilever beam, as in Fig. 3-5 has effective bending stiffness $(EI)_{\text{eff}}$ of

$$(EI)_{\text{eff}} = E_f^* I_f + E_c I_c = \frac{1}{12} w \left(E_f^* \left((2t_f + t_c)^3 - t_c^3 \right) + E_c t_c^3 \right), \tag{3.8}$$

where E_c and E_f^* represent the Young's moduli of the core, or infill, and the fiber sections, respectively; t_c and t_f represent the thicknesses of the core and infill, and w represents the width of the beam. The maximum distance from the neutral axis $y_{\max}$ is given as

$$y_{\max} = t_f + \frac{1}{2} t_c, \tag{3.9}$$

which can be used to compute the maximum strength $\sigma_{\max}$ and effective safety factor SF of the structure using

$$\sigma_{\max} = \frac{F L y_{\max}}{EI}, \tag{3.10}$$

for each material and

$$SF = \max\left(\frac{\sigma_{\text{c,yield}}}{\sigma_{\text{c,max}}}, \frac{\sigma_{\text{f,f}}}{\sigma_{\text{f,max}}}\right), \tag{3.11}$$

for the overall structure, with $\sigma_{\text{c,yield}}$ and $\sigma_{\text{f,f}}$ representing the failure stress of the core and fiber materials, respectively. In this section, we do not consider the simplified form of relative strength factor γ_{SF} given in Eq. 3.6. Instead, relative strength values are computed as $\frac{SF_i}{SF_0}$ for each design i, where SF_0 represents the effective safety factor for a uniform Nylon 6/6 beam with the same equivalent bending stiffness EI_{eff} and width w, as in Sec. 3.1.

The Young's modulus of the fiber section in Eq. 3.8, E_f^* represents an effective fiber modulus for the fiber reinforced regions. In reality, the "fiber" section is in itself a composite, where layers of fiber reinforcement alternate with layers of plastic infill, as in Fig. 3-6c. E_f^* represents the average modulus of this panel, and the fiber panel is assumed to fail at the maximum fiber strain ϵ_f. E_f^* can be computed using a rule of mixtures model [44] with fiber area fraction a_f:

$$E_f^* = E_f a_f + E_c (1 - a_f). \tag{3.12}$$

When users configure parts using Markforged's software, they are able to specify the number of fiber layers n_f, relative to the total number of layers n_t. The area fraction can be derived from these settings as

$$a_f = \frac{n_f}{n_t}. \tag{3.13}$$

Eqns. 3.8–3.13 can be combined to compute γ_{SF}, the relative strength factor, as in Sec. 3.1. Increasing the area fraction produces designs with increased relative strength (Fig. 3-7), but there is a practical upper limit to the permissible area fraction. Parts with area fractions above 0.75 are more likely to suffer from poor inter-layer adhesion or premature part failure, and they may not be manufacturable given other black-box constraints within the Markforged Eiger software. Increasing fiber provides slight improvements to relative strength (Fig. 3-8), but fiber thickness can only be set to discrete multiples of 1 mm; each 1 mm multiple represents corresponds to one concentric fiber ring. Relative strength was computed for Markforged's Nylon White with high strength high temperature (HSHT) fiberglass reinforcement for a variety of area fraction and fiber thickness values. The anticipated operating points were determined qualitatively through manufacturing parts with similar aspect ratios and sizes as a prosthetic foot.

The split, double, and triple keel geometries (Fig. 3-9 are inspired by existing commercial prosthetic feet. Many ESR prosthetic feet include a full or partial split through the keel along the sagittal plane. This feature facilitates improved coronal compliance, allowing amputees to better accommodate to uneven surfaces. The split keel cross section acts as two narrower cantilever beams, each with width $\frac{1}{2}(w - w_{\text{slot}})$, which displays the same bending behavior as one wider beam with width $w - w_{\text{slot}}$.

The equivalent bending stiffness of a beam with slot width w_{slot} and overall width w is given as:

$$(EI)_{\text{eff,split}} = \frac{1}{12}\left(E(w - w_{\text{slot}})t^3\right), \tag{3.14}$$

with $y_{\max} = \frac{t}{2}$, as in the uniform solid cross section.

While less common, some commercial prosthetic feet such as the Renegade and

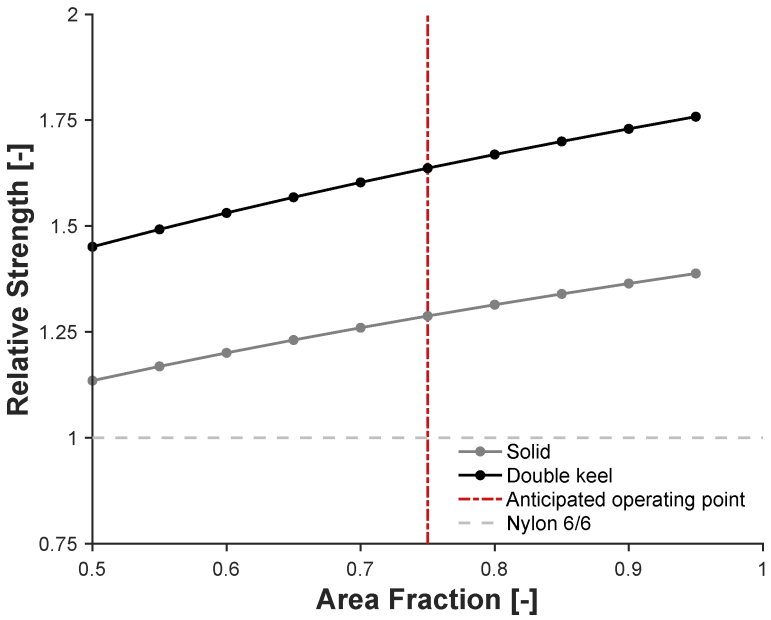

Figure 3-7: Relative strength vs. area fraction for laminated composites. Both the single (light grey) and double (dark grey) geometries show increasing relative strength with increasing fiber area fraction. In practice, area fraction is likely limited to a maximum operating point of 0.75. Data is shown for Nylon White reinforced with high strength high temperature (HSHT) fiberglass.

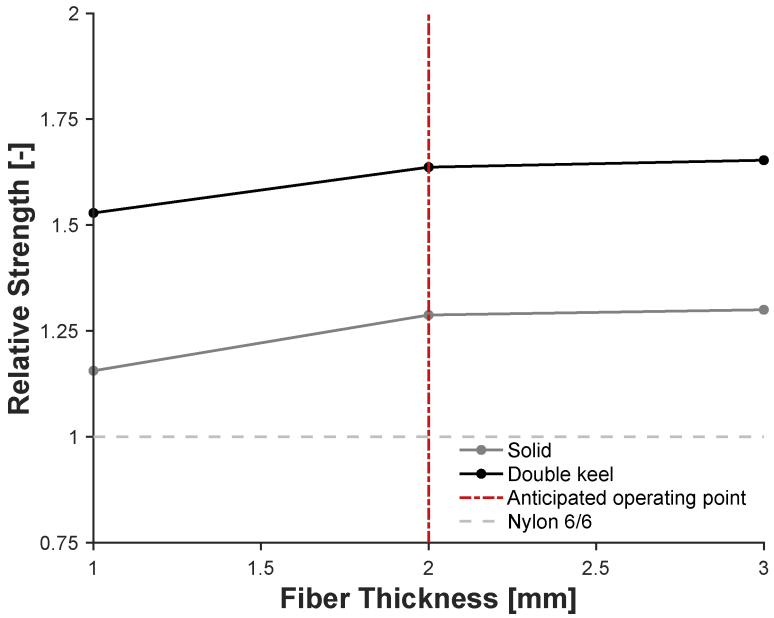

Figure 3-8: Relative strength vs. area fraction for laminated composites. Both the single (light grey) and double (dark grey) geometries show increasing relative strength with increasing fiber thickness. In practice, fiber thickness is most likely to be 2mm, which corresponds to two concentric fiber rings. Data is shown for Nylon White reinforced with high strength high temperature (HSHT) fiberglass.

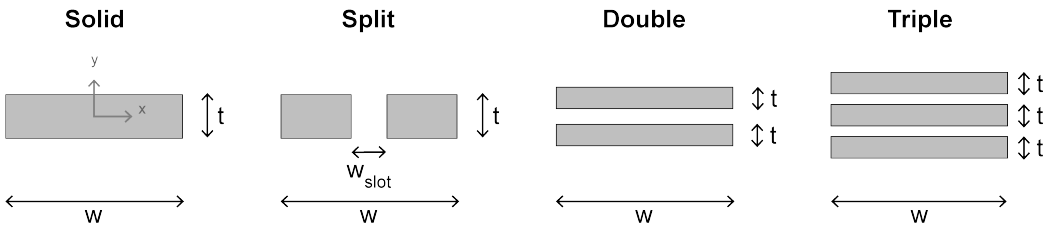

Figure 3-9: Cross sections

Thrive feet from Freedom Innovations [45] include an additional heel or keel spring. The LLTE framework has also previously been used to design multi-keel prosthetic feet [5, 19]. This additional keel or heel feature allows the prosthetic foot to have low stiffness at low loads but greater stiffness during higher impact activities. Since the beams can slide past each other, each bends about its own neutral axis. This gives equivalent bending stiffnesses $(EI)_{\text{eff}}$ of

$$(EI)_{\text{eff,double}} = 2(EI)_{\text{eff,solid}} = \frac{1}{6}Ewt^3 \tag{3.15}$$

and

$$(EI)_{\text{eff,triple}} = 3(EI)_{\text{eff,solid}} = \frac{1}{4}Ewt^3. \tag{3.16}$$

Eqns. 3.15 and 3.16 can be solved for beam thickness t to give

$$t = \left(\frac{t_0}{n}\right)^{1/3}, \tag{3.17}$$

where n indicates the total number of beams, and t_0 represents the thickness of a single beam with the same material, width, and equivalent bending stiffness $(EI)_{\text{eff}}$. Adding additional keels increases n, thus decreasing the maximum thickness t of each individual keel. As a result, a double or triple keel structure with the same equivalent bending stiffness as a single keel structure will have less strain on the outer faces of each keel. The multi-keel structure is able to bear greater stresses before failure, increasing its strength (Fig. 3-10). In this analysis, all keels in a double or triple keel structure have the same thickness, but this need not be the case.

Reinforced designs have added strength, but only if fiber is used appropriately, and only if the appropriate fiber material is selected. The Markforged CFF technology is primarily marketed as a tool for increasing strength and improving strength-to-weight ratio. Fiber-reinforced, 3D printed composites are strain-limited, and including fiber reinforcement does not necessarily improve performance for a compliant device. For the geometries relevant to this work, carbon fiber-reinforced parts are less strong than the unreinforced Nylon White material (Fig. 3-10). Fiber-reinforced fiberglass

designs, can provide improved strength relative to single-keel Nylon 6/6 designs.

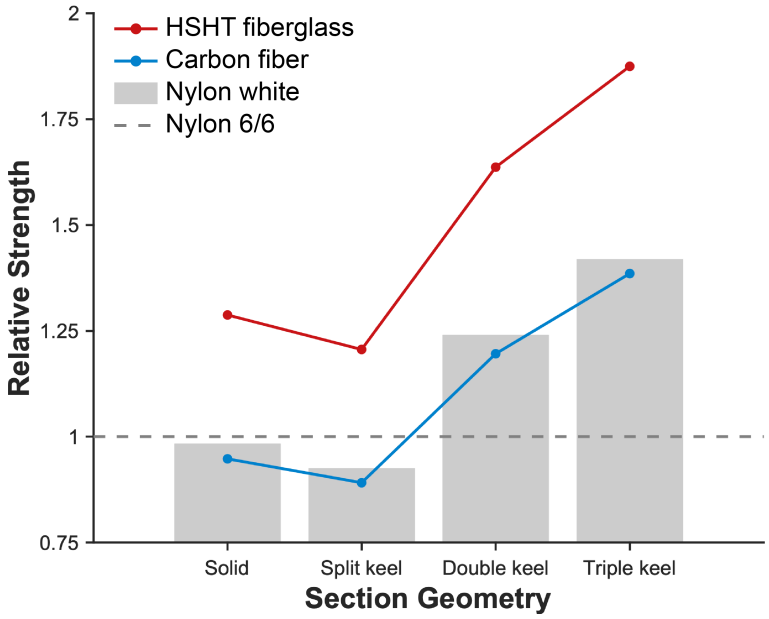

Figure 3-10: Relative strength for multiple cross section geometries. Multi-keel geometries offer improved strength capabilities for all designs, but fiber reinforcement does not universally increase strength of compliant designs; carbon fiber-reinforced designs are relatively less strong than unreinforced Nylon White designs.

3.4.3 Cost model implementation

On a high level, the total cost to manufacture a prosthetic foot, as described in Sec. 3.2.2, can be described by the material, equipment, and overhead (Eqn. 3.7). The material, equipment, and overhead costs can be further parameterized and described by process-specific inputs.

Cost of material

The material cost C_{mat} includes the cost of both raw material used to manufacture the prosthetic foot as well as wasted material. Raw materials for different manufacturing process come in different forms: Markforged CFF uses filament, while HP MJF uses powders, and CNC machining accepts solid blocks of material, which might be produced via casting or extrusion. The cost of raw material can be described as

a cost per unit volume c_{raw}. The total material cost C_{mat} also includes the cost of wasted material from scrap [1] or failed parts, which increases the effective material cost per part. The material cost can be described as:

$$C_{\text{mat}} = \frac{v_{\text{part}} c_{\text{raw}}}{(1 - \alpha_{\text{scrap}})(1 - \alpha_{\text{fail}})}, \tag{3.18}$$

where v_{part} represents the part volume. α_{scrap} represents the scrap fraction, and α_{fail} represents the part failure fraction, where $\alpha_{\text{scrap}} = 0$ and $\alpha_{\text{fail}} = 0$ represent no lost material due to scrap or part failure.

Cost of equipment

The equipment cost C_{eq} includes the cost to purchase and maintain the machines used in production. This includes the initial capital cost C_{cap} to purchase the machine, other startup costs C_{start} per machine such as shipping or installing high voltage power, and an annual maintenance cost C_{maint} for consumables and repair services. The total equipment cost C_{eq} for n_m machines and a yearly target production volume of V_{target} is given as:

$$C_{\text{eq}} = \frac{n_m}{V_{\text{target}}} \left(C_{\text{maint}} + \frac{C_{\text{cap}} + C_{\text{start}}}{\alpha_{\text{fail,machine}} t_{wo}} \right), \tag{3.19}$$

where the initial costs C_{cap} and C_{start} are linearly amortized across a write-off time of t_{wo}. During this writeoff time, α_{machine} fraction of machines are assumed to fail and need replacement. For common write-off times, α_{machine} is generally small; however, including both t_{wo} and α_{machine} as inputs to the cost model allows it to be more easily used across a range of assumed input scenarios.

The minimum number of machines $n_{m,\text{min}}$ is determined by production rates, demand, and the machine's production speed. The minimum number of machines can be described as:

$$n_{m,\text{min}} = \text{roundup}\left(\left(\frac{V_{\text{target}}}{\dot{n}_p L} \right) \left(\frac{1 + \alpha_{\text{surge}}}{1 - \alpha_{\text{fail}}} \right) \right), \tag{3.20}$$

with yearly production volume V_{target}, per-machine production rate $\dot{n}_p$, anticipated week-to-week fluctuation in product orders (demand) α_{surge}, load factor L, and α_{fail} fraction of failed parts. The load factor L represents the machine utilization rate, or what fraction of time a machine spends producing parts. $L = 1$ means the machine is used 24 hours a day, 365 days a year. In practice, this is not the case, and $L = 0.60$ is a more realistic estimation of machine utilization [30, 32].

If more manufacturing facilities n_f are desired than machines needed $n_{m,\min}$, one machine is purchased for each facility. Otherwise, the minimum total number of machines is purchased:

$$n_m = \begin{cases} n_{m,\min}, & \text{if } n_f < n_{m,\min} \\ n_f, & \text{if } n_f \geq n_{m,\min} \end{cases} \tag{3.21}$$

Cost of overhead

Overhead costs C_{overhead} include labor costs C_L for an operator to set up and attend a machine, energy costs C_E to power the equipment, and any post-processing costs C_P:

$$C_{\text{overhead}} = C_L + C_E + C_P \tag{3.22}$$

The costs to lease or purchase space for a manufacturing facility are not included. Labor costs are given as

$$C_L = S_{op}\left(\frac{t_s}{n_{ppj}} + \gamma t_p\right)\left(\frac{1}{1 - \alpha_{\text{fail}}}\right), \tag{3.23}$$

with operator hour salary S_{op}, per job setup time t_s, n_{ppj} parts per job, attendance fraction γ, and per part production time t_p. While CNC machining may produce one part per job setup, HP MJF is able to produce many parts in a single production run. t_s and n_{ppj} account for this behavior.

The cost of energy C_E represents the cost of energy consumed during production

and is given by:

$$C_E = t_p(P\dot{c}_{\text{elec}}), \tag{3.24}$$

with P power used by the machine and an electricity cost rate of $\dot{c}_{\text{elec}}$. While the cost of energy is relatively small for Markforged CFF, which uses 150 W [46], it is much greater for a four- or five-axis CNC mill, which might consume 20+ kW [47]. Some parametric models exclude energy costs if it constitutes $\leq 1\%$ of the total cost [29], and others justify its inclusion if it constitutes $\geq 1\%$ of cost [30, 32]. Including energy costs in the cost model allows parameterization across a range of machines and processes, even though energy costs will be $\leq 1\%$ in some production scenarios.

Inputs to cost model

Manufacturing costs are determined by overall production parameters as well as process-specific parameters (Table 3.3 to 3.5. In early stage design, much is still uncertain about these parameters; to capture this variability, costs were predicted across a range of parameter values. Costs were predicted for all combinations of the input parameters.

Table 3.2: Overall production parameters used for all processes

Parameter	**Levels tested**	**Justification**
Part volume, v_{part} [cm^3]	{184, 230, 276}	Representative part geometry used had volume of 233.75 cm^3. Upper and lower bounds set as ±20% volume
Number of facilities, n_{fac} [-]	{1, 5}	Hanger Fabrication Network has 10 US locations.
Surge fraction, μ [–]	{0.150}	Informal conversations with stakeholders at Hanger
Energy cost, $\dot{c}_{\text{elec}}$ [USD/kWh]	{0.0832, 0.1136, 0.1824}	Minimum, average, and maximum regional costs of industrial sector electricity [48]
Write-off time, t_{wo} [yr]	{5}	Representative write-off time from Hanger

Table 3.3: Markforged CFF-specific process parameters used as model inputs

Parameter	**Levels tested**	**Justification**
Failure fraction, α_{fail} [–]	{0, 0.05, 0.10, 0.15, 0.20}	Anecdotal experience with similar parts of similar aspect ratio and size
Replacement fraction, α_{machine} [–]	{0}	Expected machine lifespan much greater than write-off time
Parts per job, n_{ppj} [–]	{1}	One part fits in build volume at a time [46]
Per part production time, t_p [hr]	{45.6, 48, 50.4 }	Estimated time of 48 hours from Eiger. Upper and lower bounds set as ±5% of Eiger estimate
Load factor, L [–]	{0.6, 0.8, 1}	[32]
Material unit cost, c_{raw} [USD/cm^3]	{0.436, 0.500, 0.560}	Representative costs based on cost of Nylon White and HSHT fiberglass and predicted fiber volume fraction
Scrap fraction, α_{scrap} [–]	{0, 0.05, 0.10}	Fraction of material wasted at end of material spool and to print calibration parts
Machine capital cost, C_{cap} [USD]	{20000}	20000 USD purchase price for Markforged Mark Two [46]
Machine startup cost, C_{start} [USD]	{0}	Mark Two runs on standard 150W wall power [46]
Annual maintenance costs, C_{maint} [USD]	{2700}	Estimated from costs and replacement frequencies of machine components. Includes operator time to install components
Set up time per job, t_s [hr]	{0.25}	Estimated from time to upload part file and configure print in Eiger software
Post processing-cost per part, C_P [USD]	{10}	Estimated cost to tap four M6 holes for pyramid adapter mount and remove support material
Power consumption, P [kW]	{0.15}	Mark Two uses 150W power [46]
Attendance fraction, γ [–]	{0}	An operator watching a part for 15 minutes total during a 40+ hour print is negligible
Operator salary, S_{op} [USD/hr]	{15}	Representative machine operator salary

Table 3.4: HP MJF-specific process parameters used as model inputs

Parameter	**Levels tested**	**Justification**
Failure fraction, α_{fail} [–]	{0, 0.05, 0.10, 0.15, 0.20}	Anecdotal experience with similar parts of similar aspect ratio and size
Replacement fraction, α_{machine} [–]	{0 }	Expected machine lifespan much greater than write-off time
Parts per job, n_{ppj} [–]	{20, 25, 30}	Estimated 25 parts fit in fully nested build volume, per HP's Smart Stream software. Upper and lower values set as ±20% of estimate
Per part production time, t_p [hr]	{0.576, 0.640, 0.704}	Estimated time from HP SmartStream software. Upper and lower values set as ±10% of estimated value
Load factor, L [–]	{0.6, 0.8, 1}	[32]
Material unit cost, c_{raw} [USD/cm^3]	{0.130}	Representative cost of Nylon 11- or 12-based HP MJF powders
Scrap fraction, α_{scrap} [–]	{0.15}	Representative refresh rate of Nylon 11- or 12-based HP MJF powders
Machine capital cost, C_{cap} [USD]	{350000}	350000 USD purchase price for HP MJF 4200, value from informal conversations with Hanger
Machine startup cost, C_{start} [USD]	{2000}	Estimated cost to install 3-phase power
Annual maintenance costs, C_{maint} [USD]	{14000}	Estimated cost of annual service contract, value from informal conversations with Hanger
Set up time per job, t_s [hr]	{0.25}	Estimated from time to upload part file and configure print in HP SmartStream software
Post processing-cost per part [USD]	{10}	Estimated cost to tap four M6 holes for pyramid adapter mount and remove support material
Power consumption, P [kW]	{10}	Mark Two uses 150 W power
Attendance fraction, γ [–]	{0}	An operator watching a part for 15 minutes total during a 16 hour print and cooling period is negligible
Operator salary, S_{op} [USD/hr]	{15}	Representative machine operator salary

Table 3.5: CNC machining-specific process parameters used as model inputs

Parameter	**Levels tested**	**Justification**
Failure fraction, α_{fail} [–]	{0.05}	Anecdotal experience with similar parts of similar aspect ratio and size
Replacement fraction, α_{machine} [–]	{0 }	Expected machine lifespan much greater than write-off time
Parts per job, n_{ppj} [–]	{1}	Assume one part fits in workholding setup (vice) at a time
Per part production time, t_p [hr]	{0.75, 1.00, 1.25}	Estimate based on preliminary CAD/CAM toolpaths of early-stage foot geometries
Load factor, L [–]	{0.6, 0.8, 1}	[32]
Material unit cost, c_{raw} [USD/cm^3]	{0.040}	517 USD for 12"x24"x3" Nylon 6/6 extrusion (0.598 USD/in^3, 0.037 USD/cm^3). Assume recycling of Nylon 6/6 chips
Scrap fraction, α_{scrap} [–]	{0, 0.20, 0.40}	Estimates based on various amounts of chip recycling
Machine capital cost, C_{cap} [USD]	{130000}	130000 USD purchase price for Haas UMC-500 [47]
Machine startup cost, C_{start} [USD]	{5000}	Estimated cost of shipping and facility setup (3-phase power installation)
Annual maintenance costs, C_{maint} [USD]	{3500}	Yearly cost of preventative maintenance, warranty, and part replacement, from Haas annual service contract for complex mills [49]
Set up time per job, t_s [hr]	{0.25, 0.50, 0.70, 1.00, 1.25, 1.50, 1.75, 2}	Estimated 0.25 hour to setup part in machine, and range of 0-1.75 hr to configure CAM toolpaths
Post processing-cost per part [USD]	{0}	Machining costs and times included in main cost calculations
Power consumption, P [kW]	{22.4}	[47]
Attendance fraction, γ [–]	{1}	Assume full operator attendance during machining time
Operator salary, S_{op} [USD/hr]	{30}	Representative hourly salary for machinist

Impact of varying process parameters

One of the merits of a parametric cost model is its interpretability. Understanding tradeoffs related to the manufacturing process can help decision-makers navigate their decisions, and it can demonstrate the magnitude and types of uncertainty associated with the input parameters.

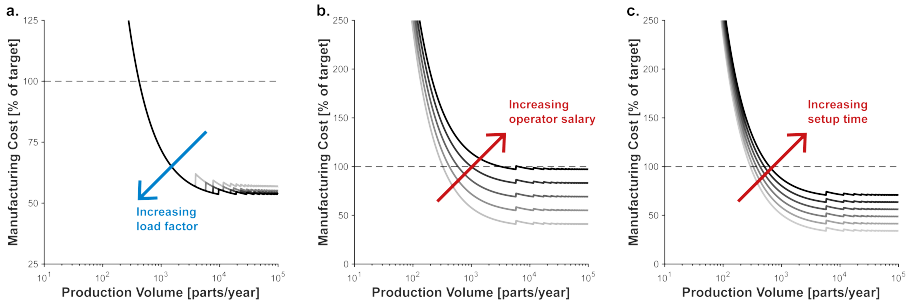

Figure 3-11: Anticipated manufacturing cost vs. production volume for CNC machining of Nylon 6/6 for a) variations in load factor, b) variations in operator salary, and c) variations in part setup time. In each graph, darker colors correspond to higher values of the varied parameter.

As described in Sec. 3.2.2, costs are primarily governed by different components in each process (Fig. 3-2 and Figs. 3-12 and 3-13). Although each Markforged printer is much less expensive than a 5-axis CNC mill or an HP MJF machine, the slow throughput means that many machines must be owned to satisfy production volume (demand) requirements.

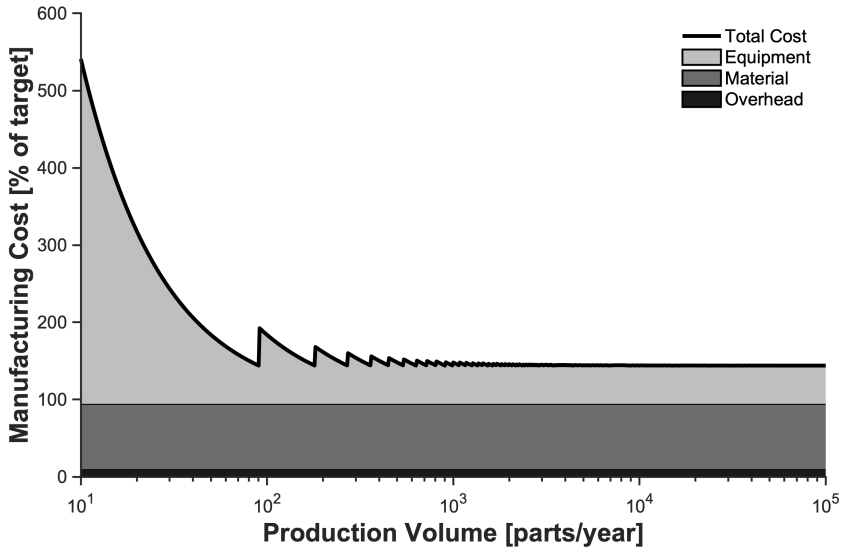

Figure 3-12: Anticipated manufacturing cost vs. production volume for Markforged CFF. Data are shown for a representative combination of model inputs, and costs are separated by component. Equipment costs (light grey) generally decrease with increasing production volume but show decaying spikes due to incremental machine purchases. At scale, the cost of Markforged CFF is driven by machine costs and expensive composite materials.

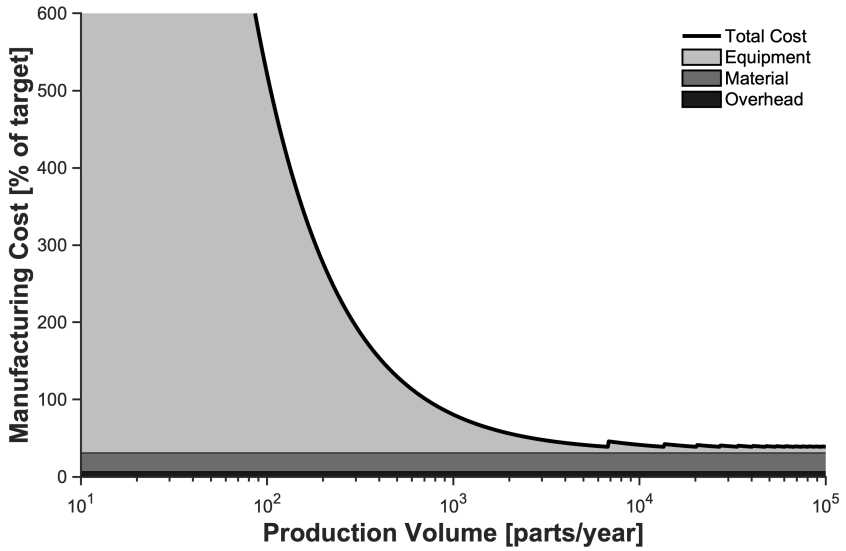

Figure 3-13: Anticipated manufacturing cost vs. production volume for HP MJF. Data are shown for a representative combination of model inputs, and costs are separated by component. Equipment costs (light grey) generally decrease with increasing production volume but show decaying spikes due to incremental machine purchases. At scale, the cost of HP MJF is driven by the cost of material.

Bibliography

[1] Michael F. Ashby. *Materials Selection in Mechanical Design*. Butterworth-Heineman, Oxford, 2 edition, 2000. ISBN 0750643579.

[2] Victor Prost, Kathryn M. Olesnavage, W. Brett Johnson, Matthew J. Major, and Amos G. Winter. Design and testing of a prosthetic foot with interchangeable custom springs for evaluating lower leg trajectory error, an optimization metric for prosthetic feet. *Journal of Mechanisms and Robotics*, 10(2):1–8, 2018. ISSN 19424310. doi: 10.1115/1.4039342.

[3] Victor Prost, W. Brett Johnson, Jenny A. Kent, Matthew J. Major, and Amos G. Winter. Biomechanical evaluation over level ground walking of user-specific prosthetic feet designed using the lower leg trajectory error framework. *Scientific Reports*, 12(1):1–15, 2022. ISSN 20452322. doi: 10.1038/s41598-022-09114-y. URL `https://doi.org/10.1038/s41598-022-09114-y`.

[4] Victor Prost, W.B. Johnson, Jenny A. Kent, Matthew J. Major, and Amos G. Winter. Sensitivity investigation of the Lower Leg Trajectory Error framework and its implication for the design and evaluation of ankle-foot prostheses (in preparation), 2022.

[5] Victor Prost, Heidi V Peterson, and Amos G. Winter. Multi-keel passive prosthetic foot design optimization using the lower leg trajectory error framework. In *ASME 2021 International Design Engineering in Technical Conferences and Computers and Information in Engineering Conference*, pages 1–14, VIRTUAL, 2021.

[6] W. Brett Johnson, Victor Prost, Pooja Mukul, and Amos G. Winter. Design and Evaluation of High-Performance, Low-Cost Prosthetic Feet for Developing Countries (in preparation), 2022.

[7] Kathryn M. Olesnavage and Amos G. Winter. A Novel Framework for Quantitatively Connecting the Mechanical Design of Passive Prosthetic Feet to Lower Leg

Trajectory. *IEEE Transactions on Neural Systems and Rehabilitation Engineering*, 26(8):1544–1555, 2018. ISSN 15344320. doi: 10.1109/TNSRE.2018.2848845.

[8] Advanced Laser Materials. Laser Sintering Material Catalog. Technical report, Advanced Laser Materials, Temple, TX, 2021. URL https://www.advancedlasermaterials.com/catalog/.

[9] Protolabs. Selective Laser Sintering PP Natural. Technical report, Protolabs, Maple Plain, MN, 2020.

[10] Protolabs. Material Comparison Guide. Technical report, Protolabs, Maple Plain, MN, 2021. URL https://www.protolabs.com/materials/comparison-guide/?query=3dprinting.

[11] Stratasys Direct. Selective Laser Sintering Materials. Technical report, Stratasys, Eden Prairie, MN, 2017. URL https://www.stratasysdirect.com/technologies/selective-laser-sintering#sls-materials.

[12] Stratasys Direct. Materials for 3D Printing Parts with FDM. Technical report, Stratasys, Eden Prairie, MN, 2017. URL https://www.stratasysdirect.com/technologies/fused-deposition-modeling#fdm-materials.

[13] Prodways Tech. 3D Printing Polymer Powders. Technical report, Prodways Tech, Merrimack, NH, 2020. URL https://www.prodways.com/en/type/plastic-powders-en/.

[14] Prodways Materials. Selective Laser Sintering Powders. Technical report, Prodways, Merrimack, NH, 2019. URL prodways.com.

[15] EOS GmbH. EOS Material Data Center. Technical report, EOS GmbH, Munich, 2020. URL https://eos.materialdatacenter.com/eo/.

[16] 3D Systems. Material Finder. Technical report, 3D Systems, Rock Hill, SC, 2022.

[17] Andrew N. Dickson, James N. Barry, Kevin A. McDonnell, and Denis P. Dowling. Fabrication of continuous carbon, glass and Kevlar fibre reinforced polymer composites using additive manufacturing. *Additive Manufacturing*, 16: 146–152, 2017. ISSN 22148604. doi: 10.1016/j.addma.2017.06.004. URL http://dx.doi.org/10.1016/j.addma.2017.06.004.

[18] Juan Naranjo-Lozada, Horacio Ahuett-Garza, Pedro Orta-Castañón, Wilco M.H. Verbeeten, and Daniel Sáiz-González. Tensile properties and failure behavior of chopped and continuous carbon fiber composites produced by additive manufacturing. *Additive Manufacturing*, 26(January):227–241, 2019. ISSN 22148604. doi: 10.1016/j.addma.2018.12.020. URL https://doi.org/10.1016/j.addma.2018.12.020.

[19] Victor Prost. *Development and Validation of a Passive Prosthetic Foot Design Framework based on Lower Leg Dynamics*. PhD thesis, Massachusetts Institute of Technology, 2021.

[20] Feras Korkees, James Allenby, and Peter Dorrington. 3D printing of composites: design parameters and flexural performance. *Rapid Prototyping Journal*, 26(4): 699–706, 2020. ISSN 13552546. doi: 10.1108/RPJ-07-2019-0188.

[21] Khalid Saeed, Alistair McIlhagger, Eileen Harkin-Jones, John Kelly, and Edward Archer. Predication of the in-plane mechanical properties of continuous carbon fibre reinforced 3D printed polymer composites using classical laminated-plate theory. *Composite Structures*, 259(November):113226, 2021. ISSN 02638223. doi: 10.1016/j.compstruct.2020.113226. URL https://doi.org/10.1016/j.compstruct.2020.113226.

[22] Anosh Amaria, Felipe Meneguzzo Pasquali, Jason N Armstron, and John F Hall. Rule of Mixtures Model to Determine the Elastic and Tensile Strength of 3D Printed Kevlar Reinforced Nylon: Theremal Gravimetric Analysis of Kevlar. In *International Design Engineering Technical Conferences and Computers and*

Information in Engineering Conference, number August, 2020. doi: 10.13140/RG.2.2.35428.73608.

[23] Ziyang Zhang, Junchuan Shi, Tianyu Yu, Aaron Santomauro, Ali Gordon, Jihua Gou, and Dazhong Wu. Predicting flexural strength of additively manufactured continuous carbon fiber- reinforced polymer composites using machine learning. *Journal of Computing and Information Science in Engineering*, 20(6):1–9, 2020. ISSN 15309827. doi: 10.1115/1.4047477.

[24] J. M. Chacón, M. A. Caminero, P. J. Núñez, E. García-Plaza, I. García-Moreno, and J. M. Reverte. Additive manufacturing of continuous fibre reinforced thermoplastic composites using fused deposition modelling: Effect of process parameters on mechanical properties. *Composites Science and Technology*, 181: 107688, 2019. ISSN 02663538. doi: 10.1016/j.compscitech.2019.107688. URL `https://doi.org/10.1016/j.compscitech.2019.107688`.

[25] Alberto Pertuz, Sergio Díaz-Cardona, and Octavio Andrés González Estrada. Fatigue in Continuous Fibre Reinforced Thermoplastic Composites. *International Journal of Fatigue*, page 130, 2020. URL `https://hal.archives-ouvertes.fr/hal-02307802`.

[26] Samuel Molony, Hadley Brooks, and Dana Tyas. Tensile and fatigue failure of 3D printed parts with continuous fibre reinforcement. *International Journal of Rapid Manufacturing*, 6(3):97, 2017. ISSN 1757-8817. doi: 10.1504/ijrapidm.2017.10003068.

[27] Francis Dantas, Kevin Couling, and Gregory J. Gibbons. Long-fibre reinforced polymer composites by 3D printing: influence of nature of reinforcement and processing parameters on mechanical performance. *Functional Composite Materials*, 1(1):1–12, 2020. doi: 10.1186/s42252-020-00010-0.

[28] Young K. Son. A cost estimation model for advanced manufacturing systems. *International Journal of Production Research*, 29(3):441–452, 1991. ISSN 1366588X. doi: 10.1080/00207549108930081.

[29] N. Hopkinson and P. Dickens. Analysis of rapid manufacturing - Using layer manufacturing processes for production. *Proceedings of the Institution of Mechanical Engineers, Part C: Journal of Mechanical Engineering Science*, 217(1): 31–40, 2003. ISSN 09544062. doi: 10.1243/095440603762554596.

[30] M. Ruffo, C. Tuck, and R. Hague. Cost estimation for rapid manufacturing - Laser sintering production for low to medium volumes. *Proceedings of the Institution of Mechanical Engineers, Part B: Journal of Engineering Manufacture*, 220(9):1417–1427, 2006. ISSN 09544054. doi: 10.1243/09544054JEM517.

[31] Douglas S. Thomas and Stanley W. Gilbert. Costs and cost effectiveness of additive manufacturing: A literature review and discussion. Technical report, National Institute of Standards and Technology, 2015.

[32] Martin Baumers, Phill Dickens, Chris Tuck, and Richard Hague. The cost of additive manufacturing: Machine productivity, economies of scale and technology-push. *Technological Forecasting and Social Change*, 102:193–201, 2016. ISSN 00401625. doi: 10.1016/j.techfore.2015.02.015. URL `http://dx.doi.org/10.1016/j.techfore.2015.02.015`.

[33] P. Dewhurst and G. Boothroyd. Early cost estimating in product design. *Journal of Manufacturing Systems*, 7(3):183–191, 1988. ISSN 02786125. doi: 10.1016/0278-6125(88)90003-9.

[34] Jong Yun Jung. Manufacturing cost estimation for machined parts based on manufacturing features. *Journal of Intelligent Manufacturing*, 13(4):227–238, 2002. ISSN 09565515. doi: 10.1023/A:1016092808320.

[35] Aini Zuhra Abdul Kadir, Yusri Yusof, and Md Saidin Wahab. Additive manufacturing cost estimation models—a classification review. *International Journal of Advanced Manufacturing Technology*, 107(9-10):4033–4053, 2020. ISSN 14333015. doi: 10.1007/s00170-020-05262-5.

[36] Karch C. Polgar, Timothy G. Gutowski, and G.W. Wentworth. Simplified time estimation booklet for basic machining operations, 1996. ISSN 09596526.

[37] Zlatan Šoškić, Gian Luca Monti, Simona Montanari, Michele Monti, and Marco Cardu. Production cost model of the multi-jet-fusion technology. *Proceedings of the Institution of Mechanical Engineers, Part C: Journal of Mechanical Engineering Science*, 235(10):1917–1929, 2021. ISSN 20412983. doi: 10.1177/0954406219837300.

[38] Douglas C. Montgomery. *Introduction to Statistical Quality Control*. John Wiley and Sons, Jefferson City, Missouri, 6 edition, 2009.

[39] Heather J. O'Connor, Andrew N. Dickson, and Denis P. Dowling. Evaluation of the mechanical performance of polymer parts fabricated using a production scale multi jet fusion printing process. *Additive Manufacturing*, 22(May):381–387, 2018. ISSN 22148604. doi: 10.1016/j.addma.2018.05.035. URL `https://doi.org/10.1016/j.addma.2018.05.035`.

[40] Max K. Shepherd, Alejandro F. Azocar, Matthew J. Major, and Elliott J. Rouse. Amputee perception of prosthetic ankle stiffness during locomotion. *Journal of NeuroEngineering and Rehabilitation*, 15(1), 2018. ISSN 17430003. doi: 10.1186/s12984-018-0432-5. URL `https://doi.org/10.1186/s12984-018-0432-5`.

[41] T. Mukherjee, W. Zhang, and T. DebRoy. An improved prediction of residual stresses and distortion in additive manufacturing. *Computational Materials Science*, 126:360–372, 2017. ISSN 09270256. doi: 10.1016/j.commatsci.2016.10.003. URL `http://dx.doi.org/10.1016/j.commatsci.2016.10.003`.

[42] International Organization for Standardization. General tolerances - Part 1: tolerances for linear and angular dimensions without individual tolerance indications (ISO 2768-1), 1989. URL `https://www.iso.org/obp/ui/#iso:std:iso:2768:-1:ed-1:v1:en`.

[43] International Standards Organization. ISO 10328:2016 - Prosthetics — Structural testing of lower-limb prostheses — Requirements and test methods, 2016.

[44] Isaac M. Daniel and Ori Ishai. *Engineering mechanics of composite materials*. Oxford University Press, New York City, 2 edition, 2006. ISBN 9780195150971. doi: 10.1016/s0261-3069(97)87195-6.

[45] Freedom Innovations. Lower Limb Prosthetic Solutions Product Catalog, 2015.

[46] Markforged Inc. Product Specifications: Mark Two, 2019.

[47] Haas Automation Inc. Quote, UMC-500, 2022. URL `https://www.haascnc.com/content/haascnc/en/build-and-price/choose-options.UMC-500.html`.

[48] U.S. Energy Information Administration. Average Price of Electricity to Ultimate Customers by End-Use Sector, 2022. URL `https://www.eia.gov/electricity/monthly/epm_table_grapher.php?t=epmt_5_6_a`.

[49] Haas Automation Inc. Preventive Maintenance Options, 2022. URL `https://www.haascnc.com/HFO/HFO-Haas_Factory_Outlet/Preventive-Maintenance.html`.

Chapter 4

Foot form: improvements to meet commercial requirements

The prosthetic feet previously created using the LLTE design framework were designed as experimental prototypes, and they did not fit into a form factor that would make them commercially accepted. As discussed in Sec. 2.2, a core user need is the ability to wear the prosthetic foot within a cosmetic foot shell and with shoes. To do this, the foot must have variable width in the frontal plane, an elevated heel, and a plantar arch. The prior single keel, single part prosthetic foot architecture presented in [1, 2] (Fig. 4-1a) was modified to include these features by introducing a new parametric description of the foot's 3-D geometry (Figs. 4-1b). The design was also modified to include a split keel to provide additional coronal compliance. While a split keel was not explicitly required from the design requirement (from Table 2.1), it enables improved adaptability on uneven terrain [3, 4] and may be preferred by K3/4 patients [4]. The constitutive model and LLTE calculations were also modified to include the added compliance of the foot shell and shoe. As in prior work, the LLTE design framework, was fully implemented in MATLAB (Mathworks, Natick, MA).

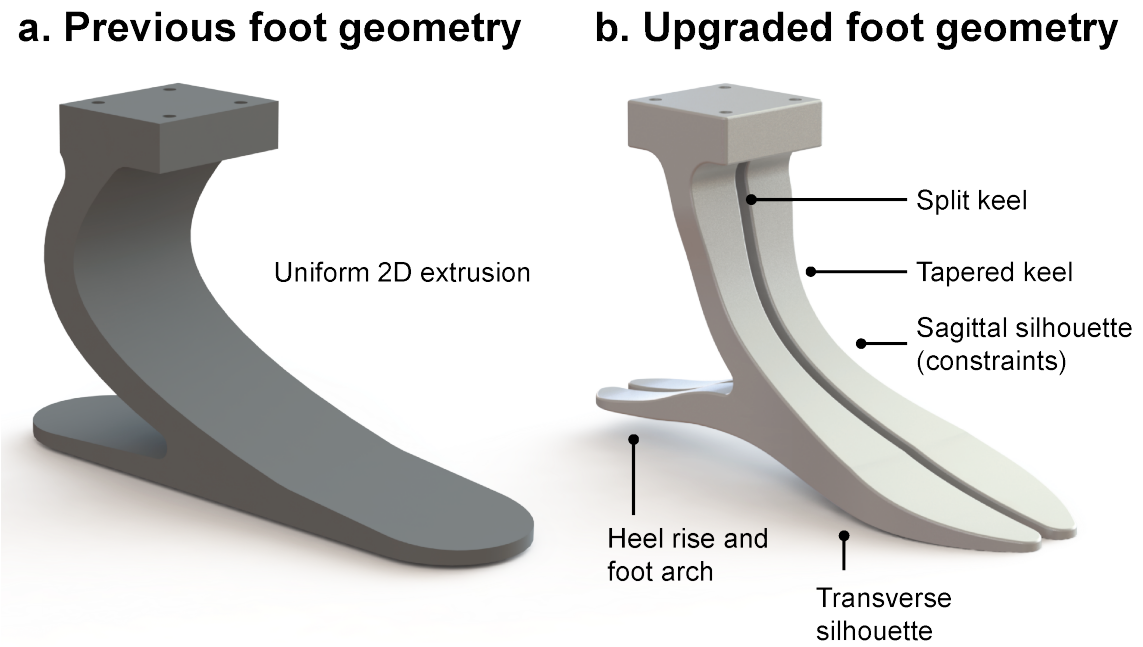

Figure 4-1: Comparison of previous and upgraded LLTE foot geometries. a) 3-D model of flat-footed LLTE foot geometry in [1, 5]. b) 3-D model of upgraded foot geometry which meets commercial form requirements to fit within a commercial foot shell.

4.1 Parametric model of foot architecture

The prosthetic foot architecture was modeled as a 3-D compliant structure using wide Bézier curves [6] and boundary curves defined by the cosmetic foot shell. Traditional topology synthesis and optimization methods often require a large number (thousands) of design variables, converge to optimal results with high stress concentrations, and suffer with manufacturability due to small feature sizes or checkerboarding patterns [7, 8]. Compared with these approaches, parametric representations such as Bézier curves or B-splines can more efficiently handle stress and manufacturing constraints [6, 9, 10]. A wide Bézier curve is a parametric curve whose shape is defined by a series of control circles; the positions of the control circles describe the shape of the curve, and the circles' diameters define the thickness of the curve. Together, the curves' shapes and thicknesses define the foot's mechanical behavaior throughout stance.

As in prior work [1, 5, 11], we described the 2-D shape and thickness of the

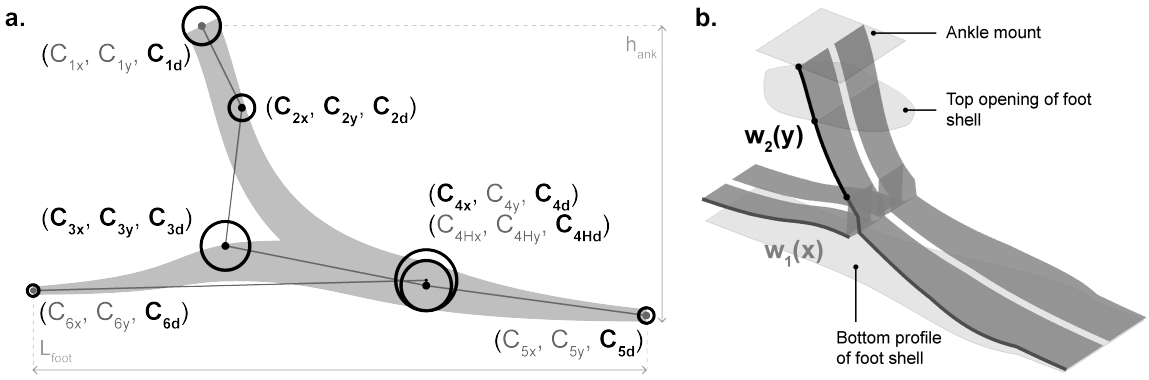

Figure 4-2: Parametric model of the upgraded foot architecture. a) The 2-D shape of the prosthetic foot is described using the Bézier curves defined by control variables C_{ij}, foot ankle height h_{ank}, and prosthetic foot length L_{foot}. The twelve independent design variables are shown in black, and the 9 dependent design variables are shown in grey. b) The 3-D shape of the prosthetic foot is described using $w_1(y)$, which defines the width of the foot below the fillet, and $w_2(x)$, which defines the width of the foot above the fillet.

prosthetic foot using a series of simpler Bézier curves joined end-to-end, known as a composite wide Bézier curve. In both the previous foot design (Fig. 4-1a [1, 5]) and the upgraded foot architecture (Figs. 4-1b, 4-2a), three wide Bézier curves are used to describe the 2-D shape of the foot. The main keel portion is represented as a cubic wide Bézier curve with control circles C_1 to C_4, the forefoot portion is represented as a linear segment with control circles C_4 and C_5, and the heel portion is described as a linear segment with control circles C_4 and C_6. Unlike the previous, flat-footed design, where the shapes of the heel and forefoot segments were defined as linear projections from a horizontal line representing the bottom of the foot, these segments are now represented as (linear) offset curves relative to a curved bottom of the foot. Here, the bottom of the foot is represented as a Bézier curve defined by the length of the foot L_{foot}, the height of heel rise h_{heel}, and the height of the arch h_{arch}; the shape of this curve is considered fixed and does not change during optimization.

The 2-D foot shape is represented with seven control circles, each of which is defined by three variables (x- and y-positions and diameter), as well as h_{heel} and h_{arch}, giving a total of 23 degrees of freedom. Of these, six were defined by the patient's foot length and residiuum length, three were coupled to another design variable, and

two were removed by fixing the center of control circle C_1 as the reference ankle-foot origin. This gave 12 independent design variables which could be tuned to describe the shape of the prosthetic foot.

The 3-D shape of the foot was defined by varying element widths along the shape of the foot. These widths were defined from 2-D cross sections of the interior of the cosmetic foot shell, at the bottom of the foot and the top opening of the foot shell, and by fixing the width at the top of the foot to w_{ankle} to 52 mm, the width of a four-hole pyramid adapter. The width of the foot at each 2-D location (x, y) is defined according to a piecewise definition,

$$w_{\text{foot}}(x, y) = \begin{cases} w_1(x) - w_{\text{slot}} & y \leq y_{\text{fillet}} \\ w_2(y) - w_{\text{slot}} & y > y_{\text{fillet}}, \end{cases} \tag{4.1}$$

where y_{fillet} represents the vertical position where the heel curve intersects the main keel curve, $w_1(x)$ and $w_2(y)$ represent the boundary curves determined by the shape of the cosmetic foot shell, and w_{slot} represents the width of the coronal plane slot in the prosthetic foot. Below the fillet, the bottom profile of the foot shell defines the width of the prosthetic foot. $w_1(x)$ represents the maximum symmetric width of the inside of the foot shell and is a function of x, the horizontal location along the bottom of the foot. Above the fillet, the side of the prosthetic foot is constrained to intersect the bottom profile of the foot shell, the top opening of the foot shell, and the ankle mount. $w_2(y)$ is defined by a cubic interpolating spline through $(y_{\text{fillet}},\ w_1(x_{\text{fillet}}))$, $(y_{\text{shell}},\ w_{\text{shell}}(x_{\text{shell}}))$, and $(y_{\text{ankle}},\ w_{\text{ankle}})$. $w_{\text{shell}}(x_{\text{shell}})$ was computed as the width of the top opening of the shell at the intersection of the Bézier curve $(x_{\text{shell}},\ y_{\text{shell}})$. This representation of the side profile both defines the 3-D foot width and implicitly constrains the 2-D foot shape to fit within the cosmetic foot shell; designs which do not pass through the top opening of the foot shell are considered geometrically invalid and do not have an associated $(y_{\text{shell}},\ w_{\text{shell}}(x_{\text{shell}}))$ The foot designs presented here were designed to fit within the Venture foot shell from College Park; however, any foot shell could be used after defining appropriate transverse plane profiles for the

top opening and plantar (bottom) surface (Fig. 4-2b, Sec. 4.4.1). Representing the 2-D shape of the foot design using wide Bézier curves and then determining the 3-D shape enables a variety of prosthetic foot designs with varying stiffness and geometry with a low number of design variables.

4.2 Constitutive model and design optimization

Prosthetic foot design using the LLTE framework requires a model to predict foot deformation and stress distribution under the anticipated loading. The foot deformation is used to calculate the LLTE metric (Eqn. 1.1) for a given design, which is used as the objective function to optimize the prosthetic foot's geometry and stiffness. The stress distribution is used to compute the effective safety factor, which acts as a constraint to ensure the strength and durability of optimized foot designs. The single-keel constitutive model in [1] was extended to accommodate the more complex foot architecture and to include the compliance of the cosmetic foot shell and shoe (Fig. 4-3). Footwear introduces additional compliance to the prosthesis and can alter its mechanical behavior [12, 13]; without incorporating this behavior, a prosthetic foot may be overly compliant when worn with shoes. The constitutive model consisted of a 2D finite element model based on frame elements [14].

As in prior work, the finite element model was build in MATLAB (Mathworks, Natick, MA), which facilitates simple and computationally inexpensive analysis, compared with commercially available structural analysis tools such as Ansys (Canonsburg, PA, USA) or SOLIDWORKS (Dassault Systèmes, Vélizy-Villacoublay, France). Although the prosthetic foot has 3-D geometry, the 2-D frame element representation facilitates a significant computational cost savings without sacrificing accuracy. A 2-D frame element has six degrees of freedom (DOF), compared with the 12 DOF of a 3-D frame element. The mesh size (300 elements) was chosen to ensure a minimal error (1%, relative to mesh sizes with an order of magnitude higher resolution) in estimated element stiffness due to the 2-D element simplification. While focusing on the kinematics and kinetics of the sagittal plane simplifies the reference walking

patterns, this is an appropriate simplification; more than 90% of the work done by the ankle during walking occurs in the sagittal plane [15]. Structural analysis occurs in the ankle reference frame, with the origin and a fixed-fixed boundary condition located at the prosthesis ankle, defined as the center of the C_1 control circle.

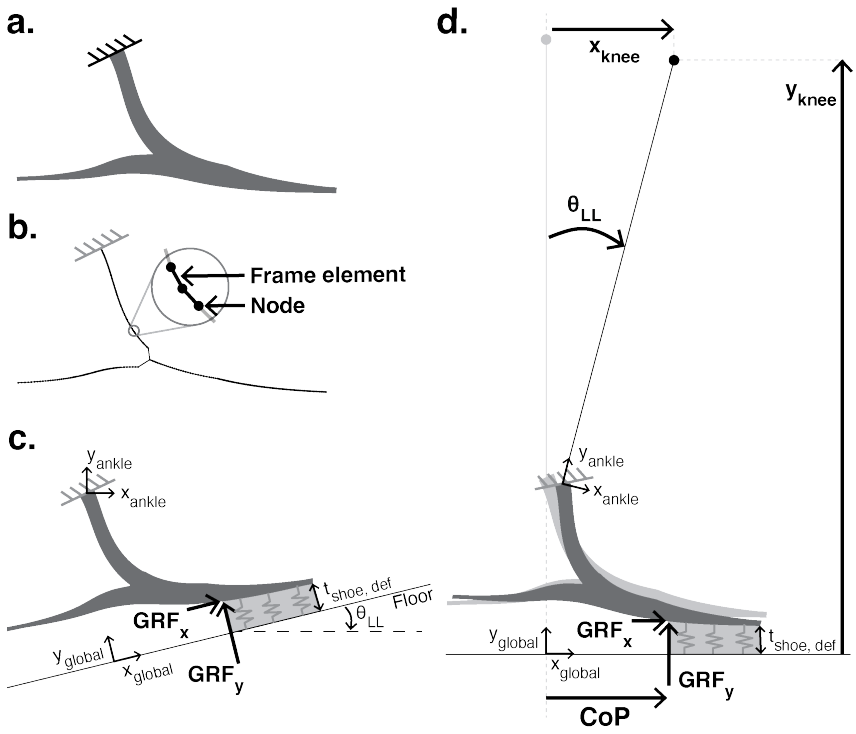

Figure 4-3: Foot-shell-shoe constitutive model. a) Prosthetic foot parametric model defined by 12 independent design variables. b) Finite element representation of the foot as frame elements. c) Deformed prosthetic foot shape and shell-shoe deformation when a set of reference GRFs are applied at a given CoP. d) Lower leg orientation and knee position resulting from the deformed prosthetic foot, cosmetic shell, and shoe. The undeformed shape (light grey) is overlaid with the deformed shape (dark grey) of the prosthetic foot, shell, and shoe.

To compute the knee position and lower leg orientation when the foot is worn within a cosmetic foot shell and shoe, the deformed thickness of these components was included in the calculations by modeling their combined stiffness as a simplified linear spring. The stiffness of the spring was determined using the geometry of the shoe at the heel and toe (approximate width, thickness, and length of engagement) and representative material properties of the foams used in shoe midsoles and cosmetic foot shells (ethyl vinyl acetate (EVA) and polyurethane (PU) foam, respectively).

4.3 Performance characterization

To demonstrate the ability of the LLTE framework to create amputee-specific prosthetic foot designs using the upgraded parametric foot architecture and constitutive model, we designed prosthetic feet for representative target amputee users with a range of body sizes (Table 4.1). A full-factorial set of target user profiles was generated based on three levels each for foot size, lower leg length, and body mass, giving a total of 27 representative users (Table 4.1). The user profiles chosen do not represent the full range of body sizes that could be used as inputs to the LLTE framework. Nevertheless, the range of foot lengths, lower leg lengths, and body masses demonstrates our capacity to design personalized feet for patients of significantly different sizes.

Table 4.1: Body size parameters used to optimize prosthetic feet for a range of target users. Feet were designed for each combination of foot size, lower leg length, and body mass, for a full-factorial, 3^3 experimental design.

Parameter	**Values**
Foot size [cm]	{25, 26, 27}
Lower leg length [m]	{0.45, 0.50, 0.55}
Body mass [kg]	{60, 80, 100}

All designs were optimized for level ground walking at a self-selected comfortable walking speed, for a minimum safety factor of at least 1.05 over level ground walking and the ISO ultimate strength loads, and for the properties of Nylon 6/6. Details of the optimization problem setup and variable bounds can be found in Sec. 4.4.2.

LLTE feet were optimized for the upgraded foot architecture (Fig. 4-4). LLTE scores using the upgraded foot architecture were much higher than those obtained using the prior mono-keel, 2-D extruded foot geometry, which were $\sim 0.05-0.06$ when designed for users of similar body size and ISO requirements [2]. This is expected due to reduced strength of the narrower 3-D foot shapes required to incorporate a slotted keel (Fig. 3-10) and to fit within the commercial foot shell. Despite this difference, all LLTE values are at or below 0.1. We have previously found that prosthetic feet which were designed for level ground walking and have an LLTE score of 0.1 or below

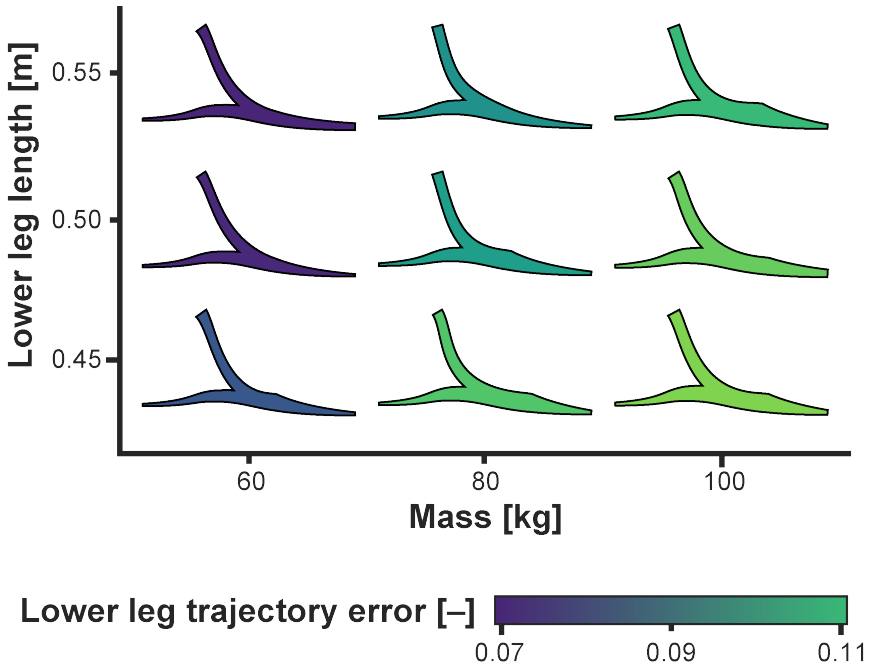

Figure 4-4: LLTE-optimal foot designs for users of a range of body sizes. Prosthetic feet optimized for size 27 cm users in a range of body masses and lower leg lengths show different geometries and LLTE scores. In general, LLTE scores are lower for lighter, taller patients.

facilitate walking performance similar to high end commercially-available carbon fiber ESR prosthetic feet [1].

With the new parametric foot architecture and upgraded constitutive model, the LLTE framework can be used to design prosthetic feet which fit into the commercial form factor, which includes a split keel, raised heel, and 3-D geometries to fit within a commercial foot shell. This foot form can be quantitatively tuned to design individualized feet for amputees of a range of body sizes, in a personalized and high-resolution way.

4.4 Supplementary information

4.4.1 Determination of permissible foot envelope

The parametric foot geometry in Sec. 4.1 requires a numeric representation of the 3-D volume the prosthetic foot can occupy within a foot shell. To fit within the shell, the

foot must closely match the profile along the bottom surface of the interior of the foot shell. If these profiles do not match well, the foot is more likely to slip or feel unstable within the foot shell. 3-D scanners are sometimes used to digitize physical and at times complex geometries. A 3-D scanner was previously used to create a computer aided design (CAD) model of the Jaipur foot for creating a ruggedized version of the LLTE foot prototypes [2, 16]. While 3-D scanners are powerful tools, they generate computationally expensive representations of geometries, often through a point cloud or mesh. Though this approach accurately represents the reference geometry, this level of detail is likely unnecessary for representing the permissible foot envelope. Additionally, 3-D scanners cannot easily represent the interior geometries of objects such as a foot shell; representing the interior geometry would require first creating an object with the geometry of the inside of the shell.

To overcome the limitations of 3-D scanning, we first generated a foam mold of the interior volume of the foot shell and then converted specific features of the shell to curve-based or parameter-based representations. A two-part elastomeric foam (FlexFoam-iT IV, Reynolds Advanced Materials, Brighton, MA) was poured inside each foot shell. After the foam set, the foam was removed, and the bottom profile of the foam was manually traced, scanned, and converted to an interpolated cubic smoothing spline within MATLAB. The top opening of the foot shell was also traced, scanned, and converted to a spline.

The interior of a foot shell is not symmetric. To overcome this and generate a symmetric prosthetic foot, the two sides (medial and lateral) of each foot shell were overlaid, and the thinner dimension at each location along the foot was used, giving the maximum permissible width of a prosthetic foot at each location along the foot. The curves for the plantar foot surface and top opening of the foot shell correspond to $w_1(x)$ and $w_{\text{shell}}(x_{\text{shell}})$, respectively (Fig. 4-2).

This process was repeated for each foot shell model and foot length considered due to nonlinear size-to-size variations in length and width. This means that foot size or shoe last grading tables, such as those in [17, 18] cannot be readily applied to representations of the foot shell geometry. These nonlinear trends likely originate from

differences he target users of each foot size; smaller feet tend to be worn primarily by women, who often wear slimmer shoes. Female feet are also often narrower in width relative to their length compared to men. If the foot shell is too loose inside of the shoe, it will slip; a relatively wider shoe will require a wider foot shell.

4.4.2 Detailed implementation of optimization problem

Optimization was performed in MATLAB using the built-in particle swarm optimization (PSO) algorithm from the Global Optimization toolbox. Prior work utilized MATLAB's built-in genetic algorithm (GA) to optimize LLTE foot designs. While GA's are excellent at navigating nonconvex, nonsmooth design spaces, they are computationally expensive. PSO is also a heuristic, population-based algorithm, but it is generally more efficient than GA [19].

Constraints and variable side bounds

The 2-D architecture of the prosthetic foot is described by the seven control circles as well as the ankle height and length of the foot, for a total of 23 degrees of freedom and 12 independent design variables (shown in Fig. 4-2a). The remaining control circle centers and diameters are defined as combinations of the independent design variables:

$$\begin{aligned} C_{3y} &= C_{4y} + \alpha_{3y} \\ C_{3d} &= \alpha_{3d} C_{4d} \\ C_{4xh} &= C_{4x} \\ C_{5d} &= \alpha_{5d} C_{4d} \\ C_{6d} &= \alpha_{6d} C_{4dh}. \end{aligned} \tag{4.2}$$

The bottom of the foot is constrained to follow a prescribed curve (in this case a wide Bézier curve). This constrains the y-positions of C_4, C_{4h}, C_5, and C_6 so that the corresponding control circles are tangent to the bottom of the foot. The length

of the prosthetic foot and the relative length of the ankle α_{heel} defines the horizontal locations of C_5 and C_6:

$$\begin{aligned} C_{5x} &= (1 - \alpha_{\text{heel}})L_{\text{foot}} \\ C_{6x} &= -\alpha_{\text{heel}}L_{\text{foot}}, \end{aligned} \tag{4.3}$$

where L_{foot} represents the length of the prosthetic foot. This number is not the same as the length of the user's physiological foot or the length of the cosmetic foot shell; L_{foot} will be smaller than both of these values so that the prosthetic foot fits within the cosmetic foot shell. The results included in this thesis used $\alpha_{\text{heel}} = 0.275$, which was set by measuring the relative heel length in existing commercial ESR feet. Adjusting α_{heel} will shift the position of the ankle origin and pyramid adapter relative to the heel and toe of the foot.

The heel and the main keel curves are connected together which leads to $C_{4x} = C_{4xh}$, as in prior work [2]. In addition, geometric constraints as in [2] were placed to prevent self-intersections which would result in geometrically invalid, non-physical structures.

Upper and lower variable side bounds (Table 4.2) were imposed on the unscaled variable values to constrain the design space to designs which approximately fit within the physiological foot form. Design variables were normalized from 0-1 for optimization according to these upper and lower side bounds. Variable normalization can be a useful technique for improving optimization performance (computational efficiency, objective value, repeatability), particularly when optimization variables x_i are of significantly different magnitudes, as is the case with C_{1d} and α_{6d}. For each evaluated design $\mathbf{x}$, the normalized optimization variables were first rescaled to generate the Bézier control variables C_{ij}. Control circle positions and diameters C_{ij} are given in m.

Table 4.2: Raw design variable bounds. Within optimization, variables were normalized by upper and lower bounds to fall between 0-1.

Design variable	Lower bound	Upper bound
C_{1d}	0.005	0.040
C_{2x}	-0.070	0.015
C_{2y}	-0.060	-0.020
C_{2d}	0.005	0.040
C_{3x}	-0.070	0.020
α_{3y}	0.001	$0.9h_{\text{ank}}$
α_{3d}	0.2	1.0
C_{4x}	0.01	0.1
C_{4d}	0.005	0.030
C_{4dh}	0.005	0.025
α_{5d}	0.2	1.0
α_{6d}	0.1	1.0

Penalized objective function

PSO does not natively handle constraints other than variable side bounds such as those in Table 4.2). To overcome this limitation and solve the constrained optimization problem, we utilized a penalty objective function $\Phi(\mathbf{x})$ instead of the original objective function $LLTE(\mathbf{x})$:

$$\Phi(\mathbf{x}) = LLTE(\mathbf{x}) + \rho \sum_{i \in I} g(c_i(\mathbf{x})), \tag{4.4}$$

where $g(c_i(\mathbf{x}))$ represents an exterior penalty function with penalty factor ρ. This formulation penalizes designs $\mathbf{x}$ which violate constraints by adding some value $g(c_i(\mathbf{x}))$ to their LLTE score. Specifically, $g(c_i(\mathbf{x}))$ was a quadratic penalty

$$g(c_i(\mathbf{x})) = \rho \max(0, c_i)^2 \tag{4.5}$$

with penalty factor $\rho = 0.5$, but $g(c_i(\mathbf{x}))$ could be replaced with a different penalty function. In the standard formulation of an optimization problem, constraints $c_i(\mathbf{x})$ are written as $c_i(\mathbf{x}) \leq 0 \ \forall i \in I$; when the constraint is satisfied, $c_i(\mathbf{x}) \leq 0$, and thus no penalty is applied.

Bibliography

[1] Victor Prost, W. Brett Johnson, Jenny A. Kent, Matthew J. Major, and Amos G. Winter. Biomechanical evaluation over level ground walking of user-specific prosthetic feet designed using the lower leg trajectory error framework. *Scientific Reports*, 12(1):1–15, 2022. ISSN 20452322. doi: 10.1038/s41598-022-09114-y. URL `https://doi.org/10.1038/s41598-022-09114-y`.

[2] Victor Prost. *Development and Validation of a Passive Prosthetic Foot Design Framework based on Lower Leg Dynamics*. PhD thesis, Massachusetts Institute of Technology, 2021.

[3] Michael Ernst, Björn Altenburg, and Thomas Schmalz. Characterizing adaptations of prosthetic feet in the frontal plane. *Prosthetics and Orthotics International*, 2020. ISSN 17461553. doi: 10.1177/0309364620917838.

[4] Björn Altenburg, Michael Ernst, P Maciejasz, Thomas Schmalz, Frank Braatz, H Gerke, and Malte Bellmann. Effects of a prosthetic foot with increased coronal adaptability on cross-slope walking. *Canadian Prosthetics and Orthotics Journal*, 4(1), 2021.

[5] Victor Prost, W.B. Johnson, Jenny A. Kent, Matthew J. Major, and Amos G. Winter. Sensitivity investigation of the Lower Leg Trajectory Error framework and its implication for the design and evaluation of ankle-foot prostheses (in preparation), 2022.

[6] Hong Zhou and Kwun Lon Ting. Shape and size synthesis of compliant mechanisms using wide curve theory. *Journal of Mechanical Design*, 128(3):551–558, 2006. ISSN 10500472. doi: 10.1115/1.2180809.

[7] Ole Sigmund and Kurt Maute. Topology optimization approaches: A comparative review. *Structural and Multidisciplinary Optimization*, 48(6):1031–1055, 2013. ISSN 1615147X. doi: 10.1007/s00158-013-0978-6.

[8] Dong Xu and G. K. Ananthasuresh. Freeform skeletal shape optimization of compliant mechanisms. *Journal of Mechanical Design*, 125(2):253–261, 2003. ISSN 10500472. doi: 10.1115/1.1563634.

[9] Yosef M. Yoely, Iddo Hanniel, and Oded Amir. Structural optimization with explicit geometric constraints using a B-spline representation. *Mechanics Based Design of Structures and Machines*, pages 1–24, 2020. ISSN 15397742. doi: 10.1080/15397734.2020.1824793.

[10] K. H. Chang and P. S. Tang. Integration of design and manufacturing for structural shape optimization. *Advances in Engineering Software*, 32(7):555–567, 2001. ISSN 09659978. doi: 10.1016/S0965-9978(00)00103-4.

[11] Kathryn M. Olesnavage, Victor Prost, William Brett Johnson, and V. G. Amos Winter. Passive prosthetic foot shape and size optimization using lower leg trajectory error. *Journal of Mechanical Design*, 140(10):1–11, 2018. ISSN 10500472. doi: 10.1115/1.4040779.

[12] Matthew J. Major, Joel Scham, and Michael Orendurff. The effects of common footwear on stance-phase mechanical properties of the prosthetic foot-shoe system. *Prosthetics and Orthotics International*, 42(2):198–207, 2018. ISSN 17461553. doi: 10.1177/0309364617706749.

[13] Matthew J. Major, Julia Quinlan, Andrew H. Hansen, and Elizabeth Russell Esposito. Effects of women's footwear on the mechanical function of heel-height accommodating prosthetic feet. *Plos One*, 17(1):e0262910, 2022. ISSN 19326203. doi: 10.1371/journal.pone.0262910. URL `http://dx.doi.org/10.1371/journal.pone.0262910`.

[14] William McGuire, Richard H. Gallagher, and Ronald D. Ziemian. *Matrix structural analysis*. Second edition, 2014. ISBN 9781507585139.

[15] Janice J. Eng and David A. Winter. Kinetic analysis of the lower limbs during walking: What information can be gained from a three-dimensional

model? *Journal of Biomechanics*, 28(6):753–758, 1995. ISSN 00219290. doi: 10.1016/0021-9290(94)00124-M.

[16] W. Brett Johnson, Victor Prost, Pooja Mukul, and Amos G. Winter. Design and Evaluation of High-Performance, Low-Cost Prosthetic Feet for Developing Countries (in preparation), 2022.

[17] Y. Luximon and A. Luximon. Shoe-last design templates. In *Handbook of Footwear Design and Manufacture*, chapter 11, pages 216–235. Woodhead Publishing Limited, 2013. ISBN 9780857098795. doi: 10.1533/9780857098795.3.216. URL `http://dx.doi.org/10.1533/9780857098795.3.216`.

[18] Y. Luximon and A. Luximon. Sizing and grading of shoe lasts, 2013.

[19] Rania Hassan, Bobak Cohanim, Olivier De Weck, and Gerhard Venter. A comparison of the particle swarm optimization and genetic algorithm. In *46th AIAA/ASCME/ASCE/AHS/ASC Structures, Structural Dynamics and Materials Conference*, Austin, TX, 2005. doi: https://doi.org/10.2514/6.2005-1897.

Chapter 5

Mechanical validation

5.1 Mechanical testing of prototype foot stiffness

To ensure that the FEA model accurately predicted the foot's deformation and thus its anticipated biomechanical performance, load-displacement curves were measured at representative locations along the bottom of a prototype prosthetic foot. Static mechanical tests were conducted using an Instron load testing machine (Instron Inc., Norwood, MA). The experimental setup consisted of a jig (Fig. 5-1) which applied loads to the foot similar to those experienced by the target user when walking on level ground at a self-selected comfortable speed. Loads were applied at representative heel ($\text{CoP}_{\text{heel}} = -30 \pm 0.1$ mm) and keel ($\text{CoP}_{\text{keel}} = 130 \pm 0.1$ mm) locations, as measured from the prosthesis ankle (Fig. 5-1). The foot was loaded at a constant rate of 300 mm/min to a maximum load $F \approx 1.2mg$, with m equal to the mass of the target user and g equal to gravitational acceleration). The vertical load (F_{instron}) and displacement (x_{instron}) were recorded at a rate of 50 Hz (Fig. 5-1), with a rated maximum force error of $\pm 6.4\%$ and displacement error of ± 0.1 mm in this configuration.

The custom jig consisted of a linear stage on which an aluminum shaft is mounted on a set of roller bearings, which reduces friction and ensures that the applied load remains normal to the bottom of the foot. Adjusting the position of the linear stage changes the location of force application along the bottom of the foot. For each prototype foot, the heel and keel loading used in the Instron testing (load location and

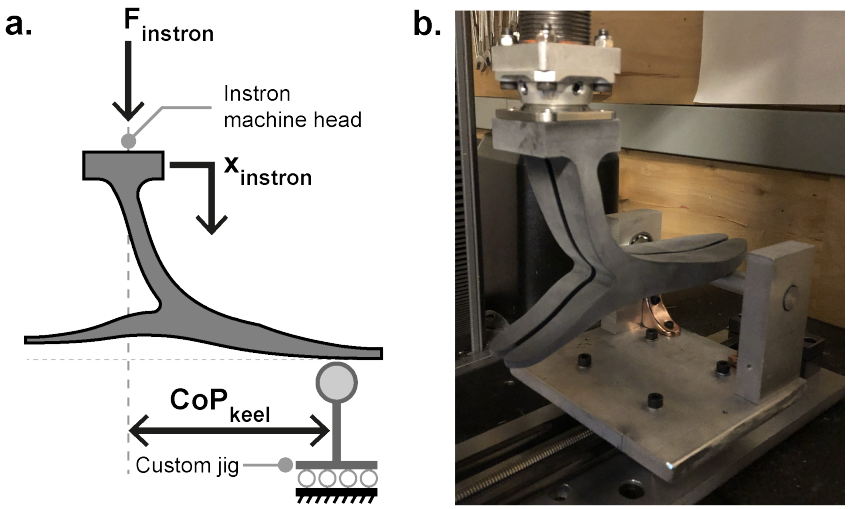

Figure 5-1: Constitutive model testing experimental setup. a) Schematic of the experimental setup, with the prosthetic foot and custom jig. b) Photograph of a prototype prosthetic foot being loaded on the Instron machine.

magnitude) was replicated using the constitutive model from the LLTE framework, giving model-predicted deformations for the prosthetic feet in each loading condition.

The prototype foot was designed for a representative user with a 26 cm foot size, lower leg length of 0.505 m, and body mass of 78.2 kg. The prototype prosthetic foot was CNC machined from Nylon 6/6 (tensile modulus $E = 2.49$ GPa, tensile yield stress $\sigma_y = 73.7$ MPa, poisson ratio $\nu = 0.6$, and density $\rho = 1130$ kg/m^3). The prototype was tested to a 920 N maximum load five times at both the keel and heel locations.

The nonlinear constitutive model accurately represented the measured deformations of the prototype prosthetic foot (Fig. 5-2). In the heel loading condition, the prosthetic foot's deformation was predicted with an average error of 0.57 ± 0.05mm relative to a measured average deformation of 4.87 ± 0.06mm, giving an $11.7 \pm 0.9\%$ average error. In the keel loading condition, the constitutive model predicted the foot's deformation with an average error of 0.27 ± 0.18mm, compared with the average measured deformation of 38.6 ± 0.3mm for an average error of $0.69 \pm 0.48\%$. The prototype foot also exhibited high energy storage and return efficiency, with an average efficiency of $87.9 \pm 3.3\%$ (Fig. 5-2). Frictional losses can be attributed to viscous dissipation in the material, not to plastic deformation or yielding.

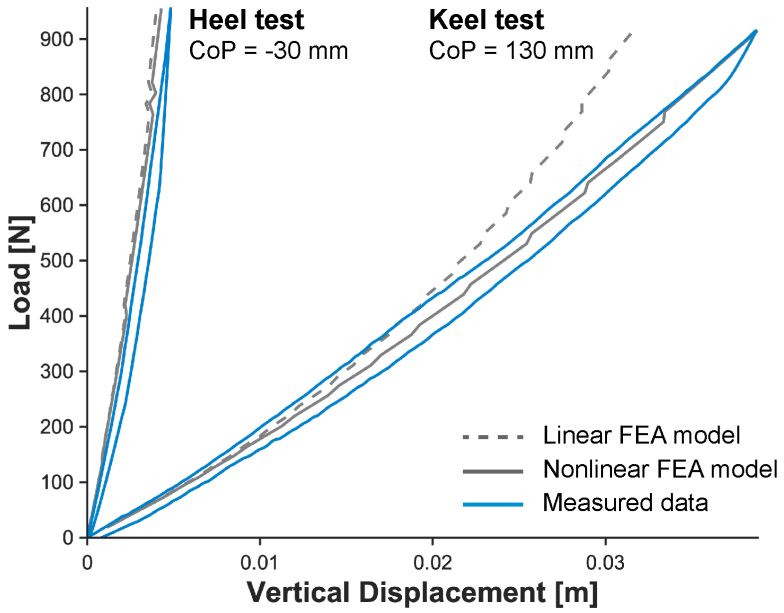

Figure 5-2: Load-displacement curve of one prosthetic foot prototype measured with the Instron machine and predicted using the constitutive structural (FEA) model. Prototypes were tested at the heel ($\text{CoP}_{\text{heel}} = -30 \pm 0.1$ mm) and keel ($\text{CoP}_{\text{keel}} = 130 \pm 0.1$ mm).

.

This testing demonstrated that the constitutive model accurately predicted the deformation of the prosthetic foot prototypes. This confirms our ability to quantitatively and predictively design prosthetic feet.

5.2 ISO ultimate strength mechanical testing

To validate that the feet passed the ISO strength tests, as they were designed to, ultimate strength static mechanical tests were conducted on a prototype prosthetic foot. Tests were conducted at both the heel and forefoot, as in ISO 10328 [1], using an Instron load testing machine. Tests were conducted at the ISO 10328 P4 level with a size 27 cm prosthetic foot designed for a representative 80 kg user.

As in our prior work [2–4], these tests were conducted using a jig which constrained the prototype foot (Fig. 5-3) at a prescribed angle while the Instron applied the corresponding ISO ultimate static test loads. Prototype feet were fixed at the required

angle (20 deg and −15 deg for the forefoot and heel conditions, respectively) and loaded on a horizontal plate with a teflon (PFTE) sheet, which minimized the shear loading, replicating the effect of the bearing-mounted platform in ISO 10328 [1]. As in the ISO 10328 protocol, feet were loaded at a constant rate of 100 N/s. The vertical load (F_{instron}) and displacement (x_{instron}) were recorded at a rate of 25 Hz, with a maximum rated force measurement error of ±2.5% and displacement measurement error of ±0.1mm. Each test was conducted twice to check for plastic deformation within the foot, which would indicate failure to pass the test.

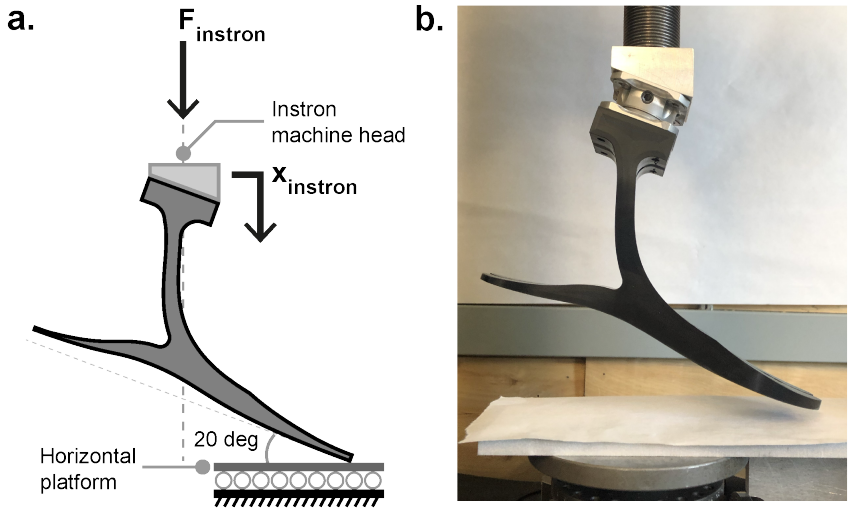

Figure 5-3: ISO ultimate static strength testing experimental setup. a) Schematic of the experimental setup. b) Photograph of a photograph prosthetic foot being loaded on the Instron machine.

The prosthetic foot prototype withstood the ultimate static tests on the Instron machine in both the heel and forefoot conditions (Fig. 5-4). The foot did not demonstrate signs of failure such as cracks, crazing, or other mechanical failures. The second test resulted in a difference in peak displacement of 0.06 and 0.14mm for the forefoot and heel loading conditions, respectively. These differences are within the measurement accuracy of the Instron machine, suggesting that the foot underwent minimal, if any, plastic deformation (Fig. 5-4).

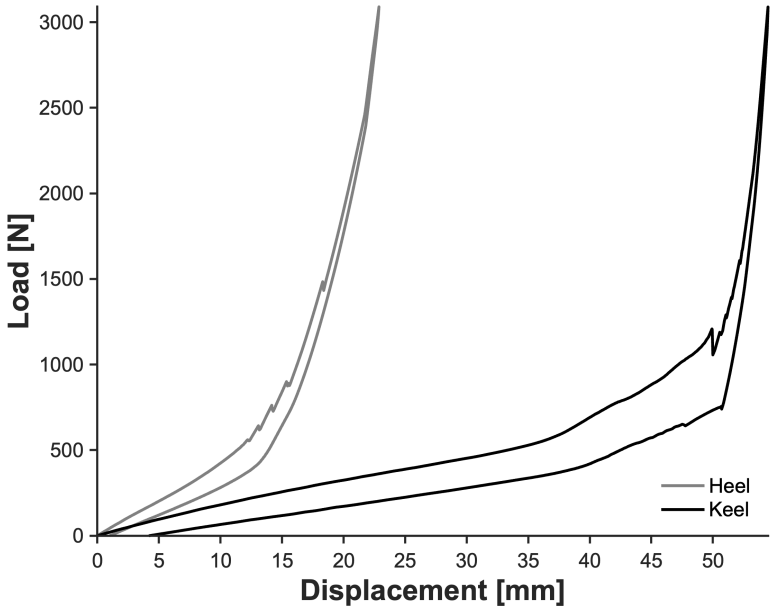

Figure 5-4: Load-displacement curves from ISO ultimate static strength testing for a prototype foot designed for an 80 kg, size 27 cm user. Per ISO 10328 [1], the prototype was loaded on the heel at a −15 deg angle and at the keel at a 20 deg angle to a maximum load of 3098 N.

5.3 AOPA dynamic heel and keel testing

To demonstrate that feet would be classified as dynamic heel, dynamic keel prosthetic feet according to the AOPA test standard [5], we conducted mechanical tests according to the AOPA standards, using a size 27 cm prosthetic foot designed for a representative 80 kg user. In each test, the prosthetic foot was attached to a pylon, which was rigidly mounted to the Instron cross head (Fig. 5-5. The foot was loaded into an aluminum plate, which was mounted to the base of the Instron and rotated to the specified angle (20 deg and 15 deg for the keel and heel conditions, respectively). As in the AOPA dynamic heel and dynamic keel protocol, the foot was loaded at a constant rate of 200 N/s to a maximum load of 1230 N. The vertical load (F_{instron}) and displacement (x_{instron}) were recorded at a rate of 25 Hz, with an estimated force measurement error of ±3% and displacement measurement error of ±0.1 mm.

To be classified as having a dynamic keel, a prosthetic foot must deform at least 25 mm under 1230 N, with an energy return efficiency of at least 75% under keel loading.

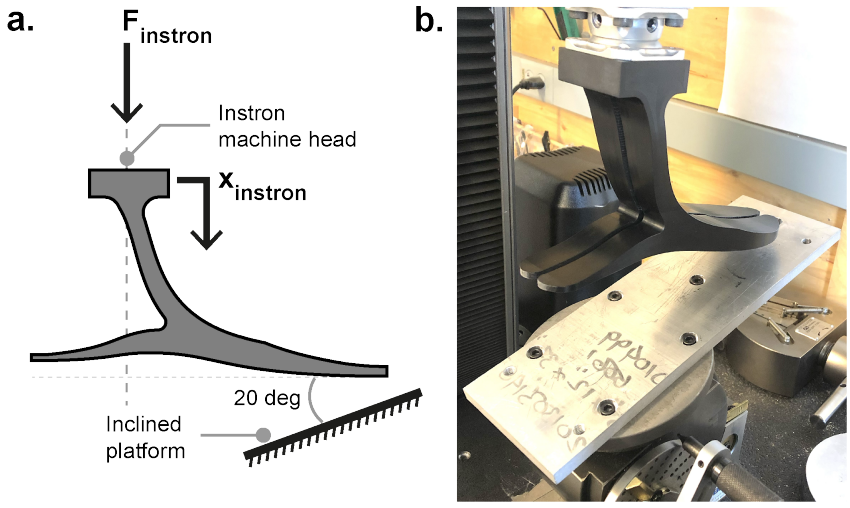

Figure 5-5: AOPA dynamic keel experimental setup. a) Schematic of test setup with prototype prosthetic foot and inclined platform. b) Prototype prosthetic foot being loaded on the Instron machine.

The prosthetic foot deformed an average of 54.2 ± 0.4 mm with an energy return efficiency of $76.4 \pm 0.2\%$ (Fig. 5-6), which satisfies this standard. For dynamic heel classification, the prosthetic foot must deform at least 13 mm or have an energy return efficiency of at least 82%. The prosthetic foot deformed an average of 17.6 ± 0.04 mm with an efficiency of $88.4 \pm 0.1\%$, passing the dynamic heel standard. By passing both the dynamic keel and dynamic heel mechanical tests, our prosthetic feet satisfy the mechanical criteria, as recommended by AOPA, to be classified as L5981 [5] (Table. 2.1).

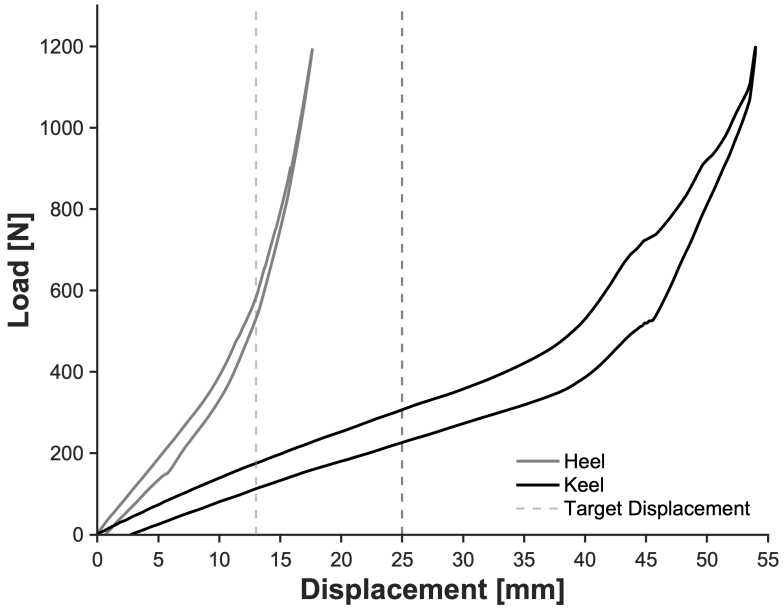

Figure 5-6: Load-displacement curves from AOPA dynamic heel and dynamic keel testing for a prototype prosthetic foot designed for a size 27 cm, 80 kg user. Per the AOPA test standards [5], the prototype was loaded to a peak load of 1230 N at both the heel (-15 deg) and keel (20 deg) platform orientations.

Bibliography

[1] International Standards Organization. ISO 10328:2016 - Prosthetics — Structural testing of lower-limb prostheses — Requirements and test methods, 2016.

[2] Victor Prost. *Development and Validation of a Passive Prosthetic Foot Design Framework based on Lower Leg Dynamics*. PhD thesis, Massachusetts Institute of Technology, 2021.

[3] Victor Prost, W.B. Johnson, Jenny A. Kent, Matthew J. Major, and Amos G. Winter. Sensitivity investigation of the Lower Leg Trajectory Error framework and its implication for the design and evaluation of ankle-foot prostheses (in preparation), 2022.

[4] Victor Prost, Heidi V Peterson, and Amos G. Winter. Multi-keel passive prosthetic foot design optimization using the lower leg trajectory error framework. In *ASME 2021 International Design Engineering in Technical Conferences and Computers and Information in Engineering Conference*, pages 1–14, VIRTUAL, 2021.

[5] American Orthotic and Prosthetic Association. AOPA Prosthetic Foot Project Report. Technical report, American Orthotic and Prosthetic Association, 2010.

Chapter 6

Discussion and Conclusions

6.1 Discussion

The focus of this thesis was to understand how to create high performance passive prosthetic feet which can be personalized for individual amputees and provided through exiting clinical methods. To do this, we envisioned a prosthetic foot solution which includes the design, manufacturing, and provision of prosthetic feet which are customized and commercially providable. In contrast to many existing ESR prosthetic feet, which cannot easily be designed in additional sizes, this enables a high-resolution sizing system and amputee-specific design.

While existing commercial ESR feet work well for many users, they are made with iterative design processes and manufacturing processes that prohibit a significant increase in the number of size and stiffness options; this leaves many users with limited walking performance and higher rates of long term overuse injuries [1–3]. Many prosthetic foot design methods in academia are also iterative and empirical, and the feet may be designed with a focus on theory, not on real-world techno-economic requirements. In this work, we identified the requirements for a high-resolution, amputee-specific personalized prosthetic foot that fits within the exiting clinical-commercial ecosystem. We created a set of core design requirements, which included economic, mechanical, and aesthetic design requirements (Table 2.1). To select an appropriate material and manufacturing method, we compared material properties as well as the

rate, cost, and quality of manufacturing processes. Using this analysis and the core design requirements, we chose a manufacturing process, CNC machining, and material, Nylon 6/6, which allowed us to best meet these needs. We also designed a novel foot form which satisfies the core design requirements, can be CNC machined from Nylon 6/6, and can be quantitatively customized through amputee-specific personalization. This foot form can be designed for a variety of user body sizes by optimizing the parametric variables which define its shape. We validated that our foot form fits within a commercial foot shell, mechanically behaves as predicted, and passes the ISO ultimate strength test, the AOPA dynamic heel test, and the AOPA dynamic keel test.

Relative to what current ESR size and stiffness systems allow, a higher level of customization in prosthetic foot design has the potential to provide both clinical and economic benefits. In prior testing of LLTE-designed feet, we found that users better replicated able-bodied walking patterns, had improved clinical outcomes such as roll-over geometries, trunk sway, prosthetic energy return, and peak push-off power, and preferred their LLTE-optimal feet, compared with a commercially-available control prosthetic foot [4] and stiffness variants of their LLTE-optimal design [5]. Improving amputee quality of life and decreasing risk of long-term injuries could also provide economic value by reducing healthcare costs due to hospitalizations, emergency room visits, and facility-based care [6].

This work builds on our prior design, mechanical validation, and clinical demonstration of the LLTE design framework. In prior work, we showed that the LLTE-designed feet can replicate biological function by accurately mimicking able-bodied kinetics and kinematics [4, 7]. Here, we demonstrated that the LLTE design framework can be used not only to produce experimental prototypes but also to design feet which meet commercial economic, mechanical, and aesthetic requirements. Satisfying these requirements enables a customized prosthetic foot to compete with existing ESR prosthetic feet, which are often made of expensive materials such as carbon fiber or fiberglass. Through a quantitative and predictive design methodology, we can meet these requirements with a lower cost but mechanically sound material, Nylon 6/6. A

prosthetic foot which can be quantitatively designed for individual users and which satisfies commercial requirements provides economic value to Hanger and fills a gap in the current product space. Some groups of users are left out with the current options. With amputee-specific prosthetic foot design, women, children, and others outside of body size and activity level norms could use better prosthetic feet for them.

Low-cost, high-performance, and customized are not mutually exclusive; with consideration of a range of stakeholder requirements and intentional design choices, they can be achieved simultaneously. Designing products for the real world requires considering a diversity of requirements. These requirements act as constraints on aspects such as how much a product may cost, how it must perform, and what form factor it must fit within. Most academic work considers one or two of these factors, but without satisfying each of these constraints, an academic prototype is unlikely to be commercially viable. Most academic work considers a subset of cost, performance, and customization, not the pursuit of all three simultaneously.

Our prior LLTE work provided insight about how to design high-performance feet for individual users using a low-cost material, but the prototypes were not designed to satisfy commercial economic or aesthetic requirements. Although powered prosthetics can be tuned for individual users or activities, customization comes through mechatronic control systems and at a steep price. In this paper, we have provided knowledge of how to design high-performance, passive prosthetic feet that satisfy economic requirements, mechanical requirements, and include the necessary features for a real prosthesis. A similar design approach could be used in related areas, including other categories of prosthetic feet, such as powered devices, running-specific feet, or modular devices which can be customized after point-of-purchase. The approach could also be horizontally translated to neighboring fields such as ankle-foot orthoses or customized footwear.

6.2 Next Steps

This thesis focused on both developing an understanding of *how* to create commercially viable, personalized prosthetic feet as well as creating and mechanically validating foot prototypes that satisfy requirements from commercial stakeholders. This work constitutes a significant step forward in the application of the LLTE design framework, bridging the gap between experimental prototypes and a mature technology ready for commercial translation and monetization. Despite this progress, additional work is needed for successful commercialization, and there remain additional knowledge gaps for subsequent research.

6.2.1 Opportunities for Future Work

These opportunities offer improved foot performance, computational efficiency, and ability to generalize the work presented here (Fig. 6-1). Improving foot performance will enable prosthetic foot designs which are stronger and more capable of replicating reference walking patterns. The existing optimization algorithm takes multiple hours to converge on an LLTE-optimal design for an individual user, which likely will not be feasible for a commercial product. To create a robust product, the LLTE-designed feet must also work well despite uncertainties in input parameters such as user body size or walking activities.

Foot performance

The performance of passive prosthetic feet is primarily a function of their material properties and geometry. The material, parametric geometry, and input user parameters define a design space of potential prosthetic foot designs. The ability to quickly and reliably identify high-performing (low LLTE) designs from this space is determined by the optimization algorithm, but the material properties and parametric foot architecture define the best-achievable performance within this space.

Together, material and geometry define the behavior of the foot throughout the stance phase and characterize how an amputee will walk in the prosthetic foot. Due

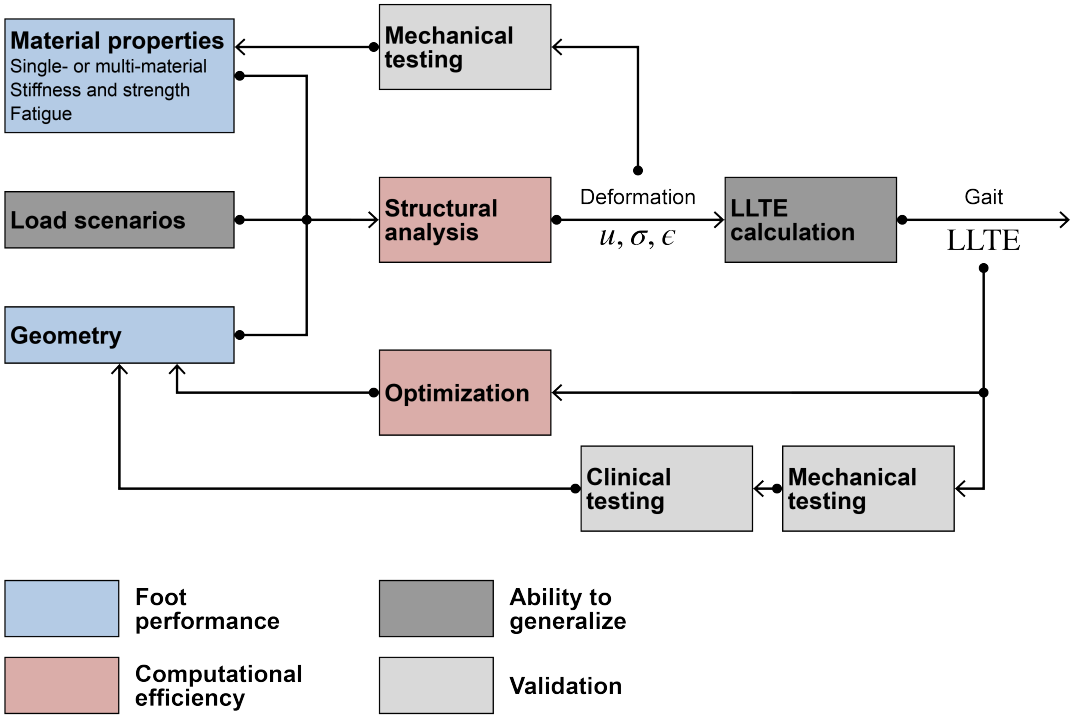

Figure 6-1: Block diagram of the LLTE design framework and associated validation and testing. Additional work could focus on improving foot performance (blue), computational efficiency (red), or the ability of the LLTE framework and LLTE-optimized designs to generalize (dark grey). Additional validation work (grey) is also necessary to validate the clinical performance and fatigue behavior of the foot designs presented here.

to narrower 3-D geometries, LLTE-optimal feet designed using the novel geometry presented in Sec. 4.3 exhibit higher LLTE values, or worse replication of reference biomechanics. Improving biomechanics further and achieving lower LLTE values will require improved material properties and/or geometry. CNC machining of Nylon 6/6 is an appropriate process given the design requirements associated with the product envisioned in this product; nevertheless, traditional composite materials such as carbon fiber or fiberglass, given the same geometric constraints, have the potential for improved walking performance.

Geometry relates not just to the 2-D or 3-D shape of the prosthetic foot but also the geometric *parameterization*, or the way the foot's shape is mathematically described. In the optimization and machine learning worlds, representation matters significantly. The current representation utilizes a 12-variable wide Bézier representation (Fig. 4-2). Despite the merits of this representation, the shape of the foot is tightly coupled to many design variables. Bézier curves are *global* polynomials, which means the shape of the curve (and the thickness of the curve, in the case of wide Bézier curves) is impacted by all control circles. In contrast, piecewise representations such as non-uniform rational basis splines (NURBS) or composite Bézier curves provide *local* control over the resulting curve. This type of local parameterization may make it easier to adjust the prosthetic foot's shape and stiffness in specific regions during optimization. Tightly coupled design variables can decrease optimization performance by making it more difficult to locate high-performing regions of the design space or to modify designs to improve performance.

Improved geometric representation could also come from a latent space representation or generative model. Instead of optimizing directly over the original design variables, it may be possible to embed the 12-variable Bézier representation within a lower-dimensional design space of latent variables. A lower-dimensional latent representation could maintain or improve the diversity of the design space and the ease (computational expense) of finding high performing designs.

Computational efficiency

Generating high performing prosthetic feet using a finite element model and heuristic optimization is computationally expensive. Evaluating prosthetic foot designs using the current linear structural analysis module is very fast; a 10-core PC can generate and evaluate 700,000 designs per hour; unfortunately, the nonlinear analysis is an order of magnitude slower but much more closely matches mechanical performance of foot prototypes (Fig. 5-2). While still much faster than commercial structural analysis tools such as ANSYS or Solidworks, better structuring the nonlinear code for computational speed would significantly reduce the computational cost of designing a personalized prosthetic foot.

The choice of optimization algorithm and its associated hyperparameters, or the settings which control the algorithm's behavior, can have a moderate impact on achievable foot performance (LLTE), computational expense (runtime), and repeatability. Switching from a genetic algorithm to particle swarm optimization improved the optimization runtime and repeatability, but other optimization or data-driven design techniques could provide further improvements.

Ability to generalize

In many fields, good designs are robust designs. Robust, generalizable designs are able to adapt well to uncertainty. For an airplane, this may mean a wing that withstands extreme weather events or higher-than-expected wind loading. For a machine learning algorithm, generalizability may mean properly classifying unseen data. In prosthetics, a robust device is one which performs well despite variations in user body size and/or walking activity.

The LLTE design framework accepts as input a prescribed set of reference walking kinetics and kinematics. These are taken from specific instances throughout stance and scaled for the desired amputee. The frames used in the current analysis were taken from prior work, which utilized a flat-footed prosthetic foot architecture [4, 5, 8]; the analysis described in [8] should be repeated to update this and select appropriate

frames for this foot architecture.

Amputees of the same body size may not require, or desire, the same stiffness prosthetic foot. Additionally, amputees may do more than walk on level ground at a comfortable speed, which was the reference activity used in this work, and user body weight is not constant but instead fluctuates day-to-day and over the course of a month [9].

Optimizing a prosthetic foot for multiple walking activities, as in [8] is one way to improve robustness and generalizability. Another technique could be to adjust input walking patterns based on amputee preference (softer, stiffer) or to explicitly design for the expected uncertainty. Instead of optimizing for *average* kinetics and kinematics, the LLTE framework could instead be used to optimize for the average walking patterns *and* the uncertainty associated with them, facilitating the creation of designs that are more robust against changes in user parameters, amputee walking pattern, and preference.

Validation

The validation in this thesis is limited to mechanical validation of the prototype prosthetic feet in static mechanical tests. This does not include fatigue testing, clinical validation, or additional mechanical testing to validate the LLTE design theory and measure the LLTE of the prototype feet.

While we have mechanically tested our prosthetic feet, additional types of testing are necessary to ensure their long-term durability and to ensure that both amputees and prosthetists like the product. In particular, future work will include mechanical fatigue testing according to ISO 10328 or 22675 as well as single-day and multi-week clinical testing with amputee users. The in-clinic testing also provides the opportunity to test the anticipated clinical provision process, which will be a focus of future work. Amputee-specific design is a powerful tool, but it must be implemented in a way that fits within prosthetists' existing prescription and workflow.

6.2.2 Remaining Knowledge Gaps

Additional commercial requirements

Further work should be conducted to explore additional requirements for commercial uptake, to test the prosthetic feet with amputee users, and to design a clinical provision process for designing and prescribing amputee-specific prosthetic feet. In this paper, we focused on the core requirements for the physical product, which included economic, mechanical, and aesthetic considerations. Other factors, such as supply chain management, marketing, and the clinical provision system will also impact commercial adoption. This work does not guarantee that the prosthetic feet will be commercially successful; nevertheless, without satisfying the core requirements, a product is unlikely to find commercial success.

Additional design features

The foot form presented here includes a split keel to facilitate improved coronal compliance. Although we included this feature and designed the foot to pass the AOPA multi-axial inversion/eversion test, there is not a quantitative understanding or consensus of how much coronal compliance is appropriate. Ongoing work from Ernst and colleagues [10, 11] is developing an understanding of both how to quantify and model coronal compliance as well as how much coronal compliance is appropriate. In future work, we hope to design for these functionalities and expand our design framework to include them.

Product provision

As product development progresses, it will be necessary to consider the experience of ordering a customized foot and to further understand the tradeoffs between the resolution of the sizing system, clinical performance, and economics. The LLTE design framework provides infinite customization ability, but this ability must be balanced with clinical benefits and economic tradeoffs. Beyond a certain resolution, creating custom product may not provide clinical benefit to amputees, but it may significantly

increase the cost and complexity of the product distribution system. A finite number of variants could meet patient needs.

Whether provision of personalized product in clinics requires a finite number of variants or requires unique prosthetic feet for individual patients, designing a foot for an individual patient will need to be fast and repeatable. This may require new computational approaches to geometric representation, calculation of a design's performance, and optimization.

Prosthetists will likely want some level of control over the optimized prosthetic foot's mechanical behavior. They are used to specifying feet by more than just a patient's body size, as they also typically consider patient preference and activity level as well; creating a prosthetist-adoptable technology may require these qualitative factors to be integrated as inputs to the foot design process or as modifications to the nominal, LLTE-optimized prosthetic foot.

Additional prosthetic foot categories

This thesis focuses on creating a single-part, L5981 prosthetic foot. Other related categories of prosthetic feet could potentially benefit from a higher level of personalization, and the LLTE framework could potentially be a way to provide this. In particular, the LLTE framework could be used to design multi-part, modular composite prosthetic feet. Many composite, modular ESR prosthetic feet already exist in industry; however, the LLTE framework could be used to quantitatively design a product line of reconfigurable components which balances the increased amputee performance of personalization with the increased manufacturing costs of creating additional tooling for composite layups.

A single- or multi-part prosthetic foot could also be incorporated a model of the behavior of other common prosthesis components. An integrated prosthesis design with vertical shock absorption or torsion components might offer additional mobility to amputees and satisfy criteria for higher insurance reimbursement levels. Additionally, transfemoral amputees use prosthetic feet primarily designed for transtibial users. A model of the knee's anticipated mechanical behavior could facilitate the

design of transfemoral amputee-specific prosthetic feet.

Prosthetists anecdotally note a lack of satisfactory K2 prosthetic feet. This work utilizes reference walking patterns from healthy and active able-bodied individuals. This may not be an appropriate reference for K2 users, who are lower mobility than the L5981, K3/K4 users of the designs in this thesis. With an appropriate set of reference data for K2 populations, the LLTE design framework could also be applied to design high-performance, low-cost K2 prosthetic feet.

Bibliography

[1] Robert Gailey, Kerry Allen, Julie Castles, Jennifer Kucharik, and Mariah Roeder. Review of secondary physical conditions associated with lower-limb amputation and long-term prosthesis use. *Journal of Rehabilitation Research and Development*, 45(1):15–30, 2008. ISSN 07487711. doi: 10.1682/JRRD.2006.11.0147. URL `http://www.ncbi.nlm.nih.gov/pubmed/18566923`.

[2] Robert L. Waters and Sara Mulroy. The energy expenditure of normal and pathologic gait. *Gait and Posture*, 9(3):207–231, 1999. ISSN 09666362. doi: 10.1016/S0966-6362(99)00009-0.

[3] Diana Zidarov, Bonnie Swaine, and Christiane Gauthier-Gagnon. Quality of Life of Persons With Lower-Limb Amputation During Rehabilitation and at 3-Month Follow-Up. *Archives of Physical Medicine and Rehabilitation*, 90(4):634–645, 2009. ISSN 00039993. doi: 10.1016/j.apmr.2008.11.003. URL `http://dx.doi.org/10.1016/j.apmr.2008.11.003`.

[4] Victor Prost, W. Brett Johnson, Jenny A. Kent, Matthew J. Major, and Amos G. Winter. Biomechanical evaluation over level ground walking of user-specific prosthetic feet designed using the lower leg trajectory error framework. *Scientific Reports*, 12(1):1–15, 2022. ISSN 20452322. doi: 10.1038/s41598-022-09114-y. URL `https://doi.org/10.1038/s41598-022-09114-y`.

[5] Victor Prost, W.B. Johnson, Jenny A. Kent, Matthew J. Major, and Amos G. Winter. Sensitivity investigation of the Lower Leg Trajectory Error framework and its implication for the design and evaluation of ankle-foot prostheses (in preparation), 2022.

[6] Dobsan DaVanzo and Associates LLC. Retrospective Cohort Study of the Economic Value of Orthotic and Prosthetic Services Among Medicare Beneficiaries Retrospective Cohort Study of the Economic Value of Orthotic and Prosthetic

Services Among Medicare Beneficiaries. Technical report, Dobsan DaVanzo and Associates LLC, Vienna, 2013.

[7] Kathryn M. Olesnavage, Victor Prost, William Brett Johnson, Matthew J. Major, and Amos G. Winter. Experimental Demonstration of the Lower Leg Trajectory Error Framework Using Physiological Data as Inputs. *Journal of Biomechanical Engineering*, 143(3), 2021. ISSN 15288951. doi: 10.1115/1.4048643.

[8] Victor Prost. *Development and Validation of a Passive Prosthetic Foot Design Framework based on Lower Leg Dynamics*. PhD thesis, Massachusetts Institute of Technology, 2021.

[9] Billie J. Randolph, Leif M. Nelson, and M. Jason Highsmith. A review of unique considerations for female veterans with amputation. *Military medicine*, 18(Suppl. 4):66–68, 2016.

[10] Michael Ernst, Björn Altenburg, and Thomas Schmalz. Characterizing adaptations of prosthetic feet in the frontal plane. *Prosthetics and Orthotics International*, 2020. ISSN 17461553. doi: 10.1177/0309364620917838.

[11] Björn Altenburg, Michael Ernst, P Maciejasz, Thomas Schmalz, Frank Braatz, H Gerke, and Malte Bellmann. Effects of a prosthetic foot with increased coronal adaptability on cross-slope walking. *Canadian Prosthetics and Orthotics Journal*, 4(1), 2021.